WILEY | Hindawi

Research Article

Finite-Element Analysis of Vertical Displacement of Laminated Rubber Bearing under Earthquake Action for Disaster Resilience of the Smart City

Denglian Yang and **Yanli Liu**

Yunnan Science & Technology Research Institute of Highway, Kunming 650000, Yunnan, China

Correspondence should be addressed to Yanli Liu; 181911805@nuaa.edu.cn

With the construction and development of smart cities, higher requirements have been put forward for the prediction and control of major natural disasters. For the prevention of earthquake disasters in super high-rise buildings, the rubber bearings of high-rise seismic isolation structures may have the risk of tensile damage in high-intensity areas, which has always been an urgent problem to be solved. In this paper, a unidirectional horizontal compression-shear experiment with 400% large deformation was conducted on the laminated rubber bearing (LNR500), and the relationship curve of vertical displacement with horizontal displacement of the bearing was obtained. According to the experimental data, an ideal elastic-plastic principal structure model was selected for the steel and a Yeoh principal structure model was selected for the rubber material, and the finite element analysis was carried out for the bearing. The time course curves of displacement, velocity and acceleration of the vertical and horizontal deformation of the laminated rubber bearing under the earthquake were obtained.

1. Introduction

The commonly used form of seismic isolation in the foundation isolation can be divided into rubber bearing, friction pendulum isolation bearing and reset spring and plane slide plate parallel system, the first two are more common [1]. Laminated rubber bearing is proposed by Kelly [2] in 1978, the bearing is formed by a layer of steel plate and a layer of rubber staggered arrangement. The vertical ultimate tensile stress of the laminated rubber bearing is much smaller than the vertical ultimate compressive stress, and the rubber bearing of the high-rise seismic isolation structure may have the risk of tensile damage and overturning in the high-intensity zone. For this reason, there are many designs and researches on the isolation tensile device [3, 4], but the effect of bearing deformation on the use of tensile devices is less considered. Especially the rubber of the bearings is mostly assumed to be incompressible material, and the vertical deformation is almost ignored, and the increase of

vertical deformation displacement of the bearing will reduce the spacing between the upper and lower flange plates, which may lead to the device failure or even damage if the tensile device does not leave enough working clearance. So, the vertical deformation of rubber bearing should be taken into consideration.

Since the 1970s, laminated rubber bearings began to be widely used, so a large number of experts and scholars conducted in-depth studies on the modeling of mechanical properties of laminated rubber bearings, large deformation cyclic response and simulation of deformation characteristics under seismic action. More classical early models such as Koh et al. [5, 6] proposed a two-degree-of-freedom model considering fluid deformation and shear deformation for simulating the effects of vertical loads on the mechanical properties of laminated rubber bearings, which assumed the contact surface as a spring model and gave insufficient consideration to the effects of damping.

The currently used intrinsic model of rubber is based on two theories [7]: one is based on the mechanics of continuous media and the other is based on a thermodynamic statistical approach. The Mooney-Rivlin intrinsic model [8] retains only the linear part and it is the simplest hyperelastic model. The Neo-Hooken and Yeoh intrinsic model [9, 10] in general it is seen as an extension of the previous form and in many cases it can be closer to the experimental data than the Mooney-Rivlin form. However, the drawback is the same, they are both linear functions and cannot describe the nonlinear behavior of rubber materials. However, the Yeoh instantonal model shows the softening phase of the rubber and can perfectly express the large deformation, so the Yeoh instantonal model is more commonly used in large deformation simulation. Ogden instantonal model [11], Ogden strain energy function with three main elongations as variables, the order N can be taken from 1 to 6, the order is too small accuracy is not enough, too large strain energy function and practical value is not much, engineering is generally used The Ogden $N = 3$ form is commonly used in engineering. The above principal structure models are widely used, such as: Wang et al. [12] improved the bidirectional coupling restoring force model for lead-core laminated rubber bearing, and used DABIS to compare the unidirectional and bi-directional seismic response of the base isolation structure of lead-core laminated rubber bearing, and the results concluded that the influence of bi-directional seismic action should be considered when determining the maximum displacement of the bearing. Ohsaki et al. [13] modeled the laminated rubber bearing with ABAQUS finite element analysis software and discretized it into hexahedral solid units, in which the Ogden hyperelastic principal model of natural rubber was selected, and simulated the deformation characteristics of the laminated rubber bearing under static and seismic effects. The Yeoh intrinsic model used in this paper is based on the method of continuous medium mechanics.

2. Laminated Rubber Bearing Mechanical Performance Test Research

The test includes two parts: the first part is the material property test of rubber and steel. In the material property test, the steel plate material is Q235 steel, the steel mainly carries out uniaxial tensile test; the rubber material carries out uniaxial tensile and pure shear test to provide the basis for the material parameters in ABAQUS; the second part is the unidirectional horizontal compression shear test of the laminated rubber bearing, which is compared and analyzed with the results of the finite element simulation analysis afterwards to ensure the reliability of the simulation data.

The laminated rubber bearing consists of flange plate, rubber layer and steel plate layer, the force subject is rubber layer and steel plate layer, flange plate mainly plays the role of connection and force transfer. Because the steel and rubber in the laminated rubber bearing is easier to deformation, so relatively speaking, the deformation of the flange plate is negligible, also has a large number of bearing simulation papers will be the flange plate as a nondeformable rigid body.

2.1. Pure Shear Test of Rubber. The density of the bearing rubber was 1.05 g/cm^3 and the initial bulk modulus K0 was 400 MPa, and the pure shear test which is shown in Figure 1 and uniaxial tensile test of the rubber were carried out in this paper. The shear test of rubber in this paper was carried out on a SANS universal material testing machine, and the gripper was loaded slowly at a speed of 50 mm/min until the specimen was damaged by loading, and the whole deformation process was recorded, as shown in Figures 2 and 3.

In this test, six rubber specimens were used, and the data were taken as the average of six tests. The rubber shear stress-strain curve is plotted in Figure 4. From the data, it can be seen that the stress-strain curve is close to a straight line when the horizontal strain is less than 250%; when the horizontal strain is greater than 250%, the rubber has an obvious period of stiffness strengthening; and when the horizontal strain reaches 450%, the specimens are damaged. Because simple shear can be seen as pure shear plus rotation [14], therefore, at strains greater than 250%, the principal stress of the shear ellipse within the rubber is skewed, and the rubber is subjected to shear in addition to tensile, so that the apparent strength increase can be seen only at a later stage.

2.2. Rubber Uniaxial Tensile Test. The tensile test of rubber in this paper was carried out on SANS universal material testing machine, as shown in Figure 5. The rubber tensile specimens should be dumbbell-shaped as shown in Figure 6. The number of specimens is 3. The width of the narrow part are 6.01 mm; the thickness are 2.35 mm, 2.26 mm, 2.28 mm; the length is 33 mm; the lead gauge clamping spacing is $l_o = 25$mm.

The test results were taken as the average of three test results. The rubber tensile stress-strain curve is plotted in Figure 7. From the test, it can be seen that the ultimate tensile strength of the rubber is 21.84 MPa and the ultimate tensile strain is 738%; the rubber monotonic tensile curve is nonlinear, its elastic modulus is variable, the initial elastic modulus is about 1 MPa, and the later strength is obviously higher than the earlier one.

2.3. Uniaxial Tensile Test of Steel. The instrument used in this test is an electronic universal testing machine, and the strain rate during yielding of the metal material should be determined between 0.00025/s and 0.0025/s. Plate thickness, tensile area, elongation gauge clamping spacing. Width of both ends of the specimen, width of the narrow part of the specimen. The shape of the test piece and test photo are shown in Figures 8 and 9. Based on the dimensional information, the loading rate can be calculated as follows:

$$\begin{aligned} u &= l\varepsilon_e \\ &= 120 \times 0.00025 \sim 0.0025 \times 60 \\ &= \frac{1.8 \sim 18mm}{\text{min}}. \end{aligned} \tag{1}$$

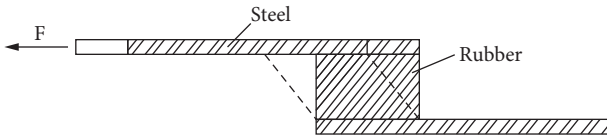Therefore, the test loading rate of 2 mm/min. test temperature for the room temperature, the number of test pieces

FIGURE 1: Pure shear test rubber specimen force mode.

FIGURE 2: SANS universal material testing machine.

FIGURE 3: Rubber test piece and steel plate connection diagram.
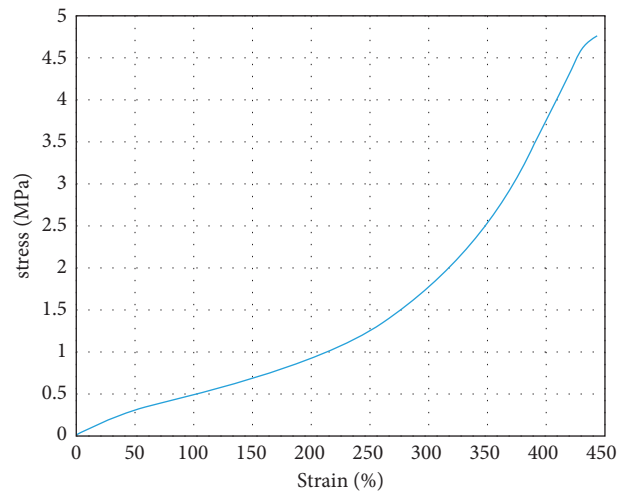
FIGURE 4: Graph of rubber shear stress-strain curve.

a total of 3. Steel and laminated rubber bearing steel plate layer is the same, are Q235 steel.

The results were taken as the average of three tests and the results are shown in the Table 1.

2.4. Bearing Horizontal Compression Shear Test. The test object is a 500 mm diameter laminated rubber bearing (LNR500), and the main monitoring data are, under the compression shear state, the lateral displacement, vertical displacement and horizontal force of the bearing. The variables controlled by the tester are horizontal displacement and vertical pressure. In the test of 400% limit shear, bearing top surface pressure is 12 MPa and the number of test bearing is 3. The test machine for this experiment is 1500 t electro-hydraulic servo compression shear test machine (FJS1W5001) as shown in Figure 10. When doing 400% large deformation, 4 displacement gauges were evenly arranged around the bearing, and the displacement gauges were adsorbed under the upper flange plate, which could move with the flange plate movement, and the displacement gauges were kept perpendicular to the lower flange plate when moving, as shown in Figures 11–13.

The data of bearing reaction force and bearing transverse displacement can be read from the monitoring data inside the testing machine, and the bearing vertical displacement is read from the monitoring data of displacement meter, and the data is collected once every 0.02 s interval. The test adopts the way of controlled displacement, the maximum displacement reaches 377 mm. the data is taken from the average of 3 bearing test data.
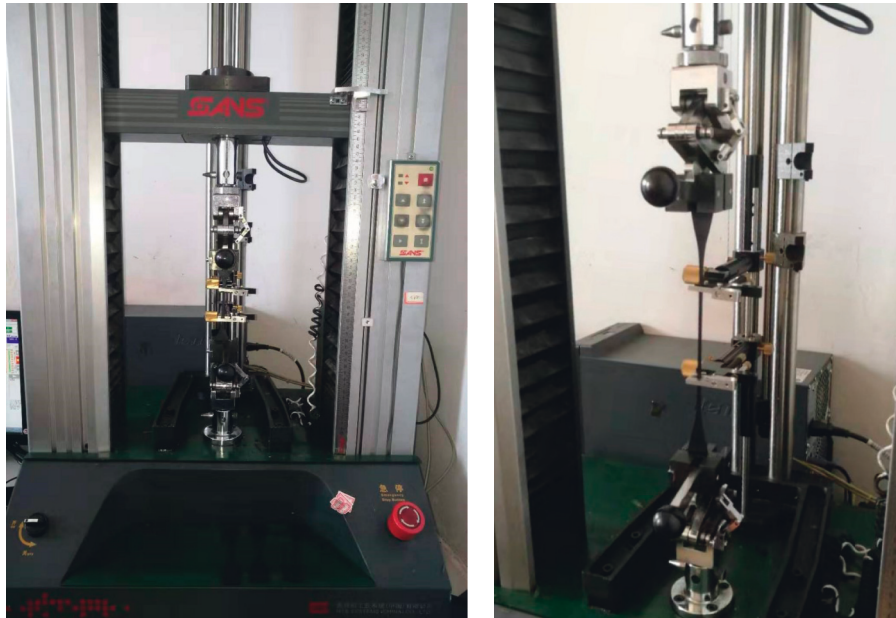
(a)   (b)
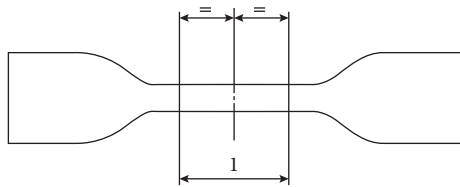
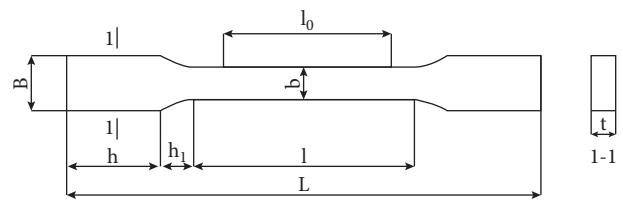FIGURE 5: Graph of rubber tensile test.

FIGURE 6: Dumbbell-shaped specimen shape.
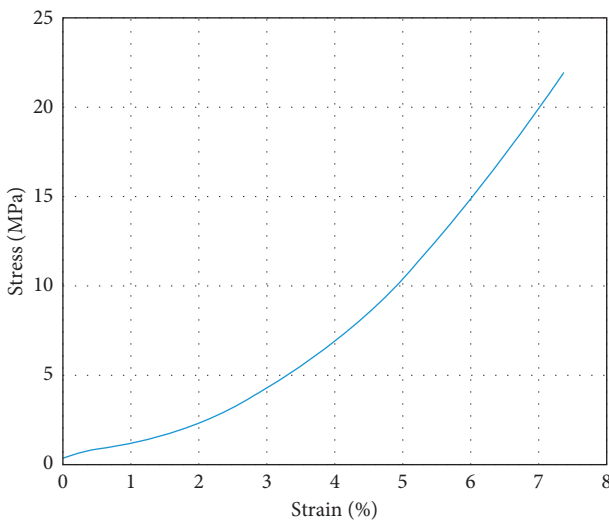

FIGURE 8: Diagram of the plate strip head specimen.

FIGURE 7: Graph of rubber tensile stress-strain curve.

stage of the rubber bearing, this stage of the press shear slowly apply pressure until the bearing upper pressure reaches 12 MPa, then keep the pressure onstant and shear the bearing. In the static pressure stage, the height of the bearing vertical drop is 2.89 mm on average, and with the increase of lateral displacement, the pressed area is reduced from a whole circular surface to a shuttle-shaped area.

If we set the lateral displacement as X and the bearing diameter as R, we can deduce the formula of shuttle area as follows:

$$S = 2R^2 arccos\left(\frac{x}{2R}\right) - x\sqrt{R^2 - \frac{x^2}{4}}. \tag{2}$$

As can be seen from Figures 14 and 15, after the horizontal displacement reaches the maximum, the vertical drop height of the bearing is 9.55 mm, the thickness of the rubber layer is 92.96 mm, and the drop percentage is 10.27%, which is negligible compared with the whole floor, but this displacement is not negligible compared with the tensile device set in the seismic isolation layer. Because as the displacement increases, the vertical load remains unchanged, but the compressed area becomes smaller, as shown in the Figure 16. So accordingly, the

In the graph of the relationship between horizontal displacement and vertical displacement, it can be observed that when the horizontal displacement is 0, there is a section of displacement vertical change section, this section is the beginning of the test, the static pressure

FIGURE 9: Steel tensile test.

TABLE 1: Steel tensile test data sheet.

Specimen number	Yield strength (MPa)	Tensile strength (MPa)	Elongation (%)	Elastic modulus (MPa)
1	288.1	458.2	25.3	201400
2	281.7	431.6	29.8	198300
3	302.5	439.4	30.0	196000
Average value	290.8	443.1	28.4	198567

FIGURE 10: Field test setup diagram.
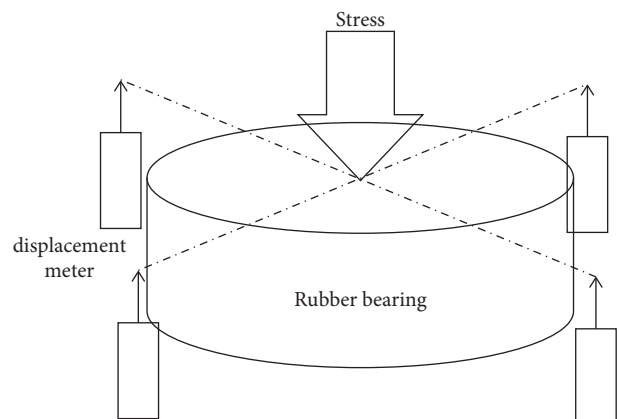
FIGURE 11: Schematic diagram of the relative position of the displacement meter and the bearing.

vertical stiffness will be reduced, so the vertical displacement is produced. Therefore, the rubber cannot be simply regarded as incompressible material in the finite element simulation.

The vertical pressure is 12 MPa, then the upper pressure can be calculated as 2355 kN. Converting the test results into the relationship between displacement and stiffness, then the relationship curve are plotted in Figures 17 and 18.
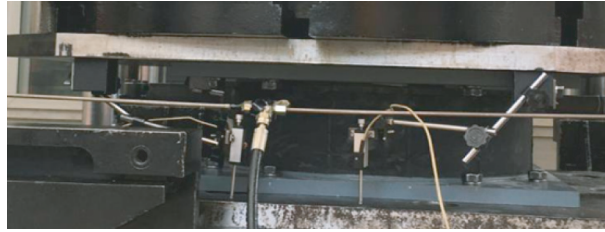
FIGURE 12: Schematic diagram of the installation of the bearing and displacement meter.
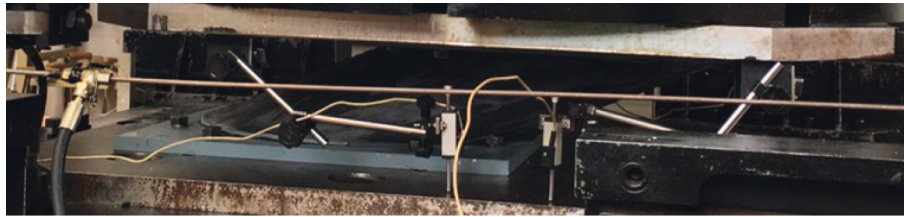

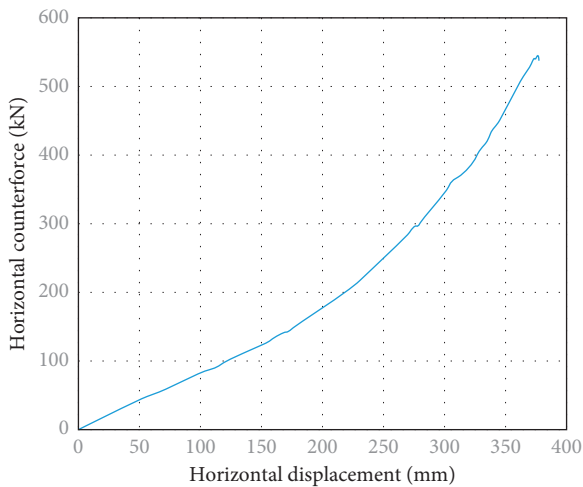FIGURE 13: 400% ultimate shear bearing deformation diagram.

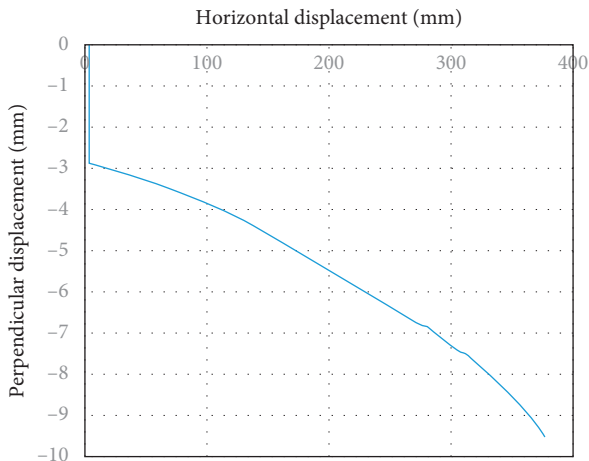FIGURE 14: Relationship between horizontal reaction force and horizontal displacement of LNR500.

FIGURE 15: Relationship between vertical displacement and horizontal displacement of LNR500.
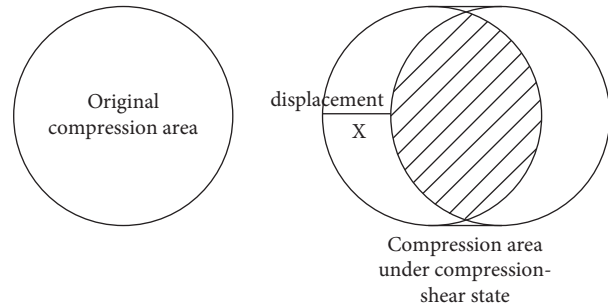

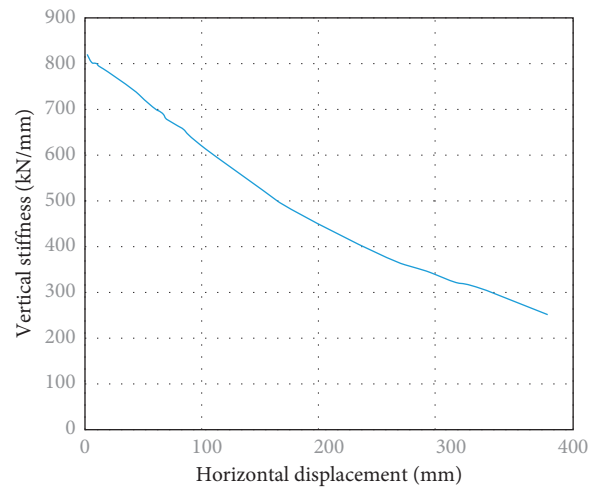FIGURE 16: Bearing compression shear state under pressure area reduction.

FIGURE 17: Relationship between vertical stiffness and horizontal displacement.

The initial vertical stiffness of the laminated rubber bearing LNR500 is 814.88 kN/mm, with the increase of horizontal displacement, the vertical stiffness decreases, when the horizontal deformation reaches 100%, the vertical
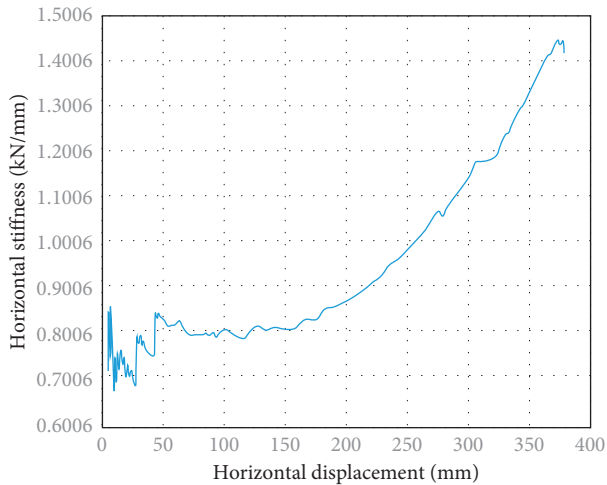
FIGURE 18: The relationship between horizontal stiffness and horizontal displacement.

stiffness is 620.83 kN/mm, down 23.74%; when it reaches 200%, the vertical stiffness is 449.72 kN/mm, down 44.74%; when it reaches 300%, the vertical stiffness 342.46 kN/mm, a decrease of 57.97%; when reaching 400%, the vertical stiffness is 246.48 kN/mm, a decrease of 69.75%. It can be seen that the vertical stiffness decreases faster, but its magnitude decreases with the increase of horizontal displacement, and the rate of decline in the later period is slower than that in the earlier period.

Since the horizontal reaction force data read by the press shear is more shaky during the experiment, the relationship curve between horizontal stiffness and horizontal displacement also fluctuates somewhat. The initial horizontal stiffness is about 0.8 kN/mm; when the deformation reaches between 100% and 200%, the horizontal stiffness changes slowly and even has a decreasing trend, the lowest is about 0.79 kN/mm; when the horizontal displacement reaches 377 mm, that is, when 400% limit shear displacement is reached, the horizontal stiffness is the largest, reaching 1.4 kN/mm.

3. Bearing Finite Element Static Simulation

3.1. Bearing Finite Element Modeling. The bearing studied in this paper is a lead-free core laminated rubber bearing (LNR500). The thickness of each layer of steel plate is 3 mm, 15 layers in total; and the thickness of each layer of rubber is 5.81 mm, 16 layers in total, as shown in Figure 19. The middle of this bearing is hollow, the aperture is 80 mm. there is a thin layer of rubber around the bearing as a protective layer, because it does not participate in the force analysis, the flange plate mainly plays the role of connection and force transfer, compared with the rubber and steel plate, its deformation is negligible, so the simulation are discarded. The contact surface of the rubber layer and steel plate layer of the bearing model is chosen to bind the connection as shown in Figure 20.

This laminated rubber bearing is made of Q235 steel with an elastic modulus of $E = 198567$ MPa, Poisson's ratio $\mu = 0.25$, yield strength = 290.8 MPa, tensile strength = 443.1 MPa, and elongation $\delta = 28.4\%$. The ideal elastic-plastic intrinsic model is chosen for the simulation of steel in this paper as shown in Table 2.

In this paper, the Yeoh intrinsic structure model is chosen for the rubber material. The Yeoh model parameters were obtained from the experimental results. Although the usual value is negative because it mainly describes the state of rubber in the softening stage, the softening of rubber in this paper is not obvious enough, so it is positive. Parameter settings are shown in Table 3. The density of rubber is 1.05 g/cm3.

According to the test process data of 400% ultimate shear, the upper pressure should be 12.06 MPa. U2 that is, the Y-direction displacement is 377 mm.

4. Analysis Results and Comparison

Observation of the resultant stress clouds reveals that:

(1) As can be seen from Figure 21, initially in the pure pressure state, the vertical displacement of all parts of the bearing is 0. All units in the bearing are in compression, and the relative displacement of the upper unit of the bearing is the largest, 2.89 mm.

(2) As can be seen from Figure 22, when the horizontal displacement reaches 75 mm (when the horizontal shear reaches 81.5%), the left lower part of the bearing has a more obvious unit with positive vertical displacement, at this time the bearing should be in local tension, and after reaching 150%, the bearing is in tension very obviously.

(3) As can be seen from Figure 23, when the 400% ultimate compression shear state is finally reached, the number of units with positive vertical displacement in the left half of the bearing increases significantly, and the tensile area inside the bearing is larger at this time.

In the previous section, it was also mentioned that there is local tension inside the bearing in compression shear state, which is partly responsible for the increase in horizontal stiffness of the bearing, and this resultant diagram also corresponds to this statement. The stress cloud diagram of the middle layer unit of the bearing is as shown in Figures 24–29. There is a relatively obvious stress concentration in the middle where there is a hole, from the diagram it is also obvious to observe the location of the middle compressive zone, which is a shuttle-shaped area. S11, S22, S33 are positive values of tensile stress, from the diagram it is also obvious to observe the local tensile situation.

The data monitored in the test are the horizontal displacement of the upper part of the bearing, the horizontal reaction force and the vertical displacement of the height drop of the bearing. In order to make the simulation results correspond to them, in the course output, the horizontal displacement (Y direction), horizontal reaction force (Y direction) and vertical displacement (Z direction) of the upper surface of the bearing are selected to be output. After

(a)   (b)
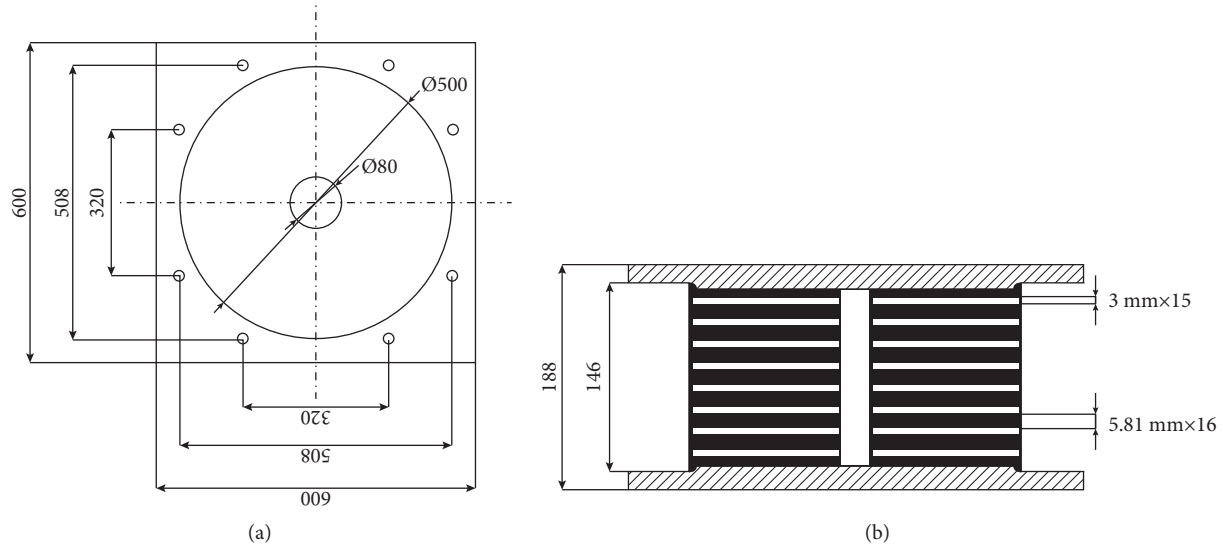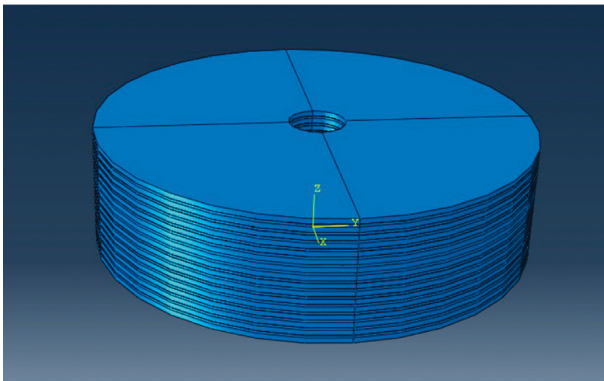
FIGURE 19: Dimensional drawing of LNR500.

FIGURE 20: Geometric model of LNR500 in ABAQUS.

TABLE 2: Relationship between stress and plastic strain in steel.

Real stress (MPa)	Plastic strain
291	0
443.1	1

TABLE 3: Table of parameters of the Yeoh model for rubber materials.

C10	C20	C30	D1	D2	D3
0.23	0.0013	0.000176	0.00504	0.005	0.000005

processing the obtained simulation data, the following curve is obtained. Compare the simulation result with the test result data curve.

The relationship curves of horizontal reaction force and horizontal displacement are in good agreement. Simulation results of vertical displacement: at the initial compression stage, the test data is 2.89 mm and the simulation data is 2.90 mm; when the lateral displacement reaches 377 mm, the test data is 9.54 mm and the simulation data is 9.81 mm; the maximum error of the intermediate data is 8.91%, not more

than 10%, and the vertical displacement-horizontal displacement relationship curve matches well. In the test, when the press shear pushes the upper part of the bearing to produce horizontal displacement, the pressure exerted on the upper part of the bearing cannot be kept completely consistent, so the error within 10% is within the allowable range. Then the test data derived from the simulation is further converted into the relationship between stiffness and displacement, and the comparison is as shown in Figures 30–33.

The finite element simulation shows the characteristics of the change of stiffness of the rubber bearing in three different stages. The starting bearing stiffness is low, 0.7 kN/mm. In the actual project, the equivalent horizontal stiffness is taken as the corresponding shear stiffness at 100% deformation, 0.81 kN/mm. In the middle deformation, there is a softening stage, and its stiffness change has a plateau period. The horizontal stiffness is 1.4 kN/mm when 400% ultimate deformation is reached.

The change curve of vertical stiffness is more linear compared with horizontal stiffness, and the initial vertical stiffness and the vertical stiffness at 400% are basically consistent with the test results. In the middle deformation, there is a slight difference due to the relationship of the error of the test itself and the influence of the simulation error, but the error at the maximum error between the simulation data and the test data in this paper is 9.09%, not more than 10%, and it is still considered to be in good agreement.

5. Bearing Finite Element Dynamic Simulation

5.1. Finite Element Simulation of the Bearing under Seismic Action. The structure chosen in this paper is an asymmetric L-shaped structure, and the structural form of this project is determined to be cast-in-place concrete frame structure. The horizontal displacement of the bearing is generally not more than 250% of the thickness of the bearing rubber layer for a building with few floors. Within this range, the calculation
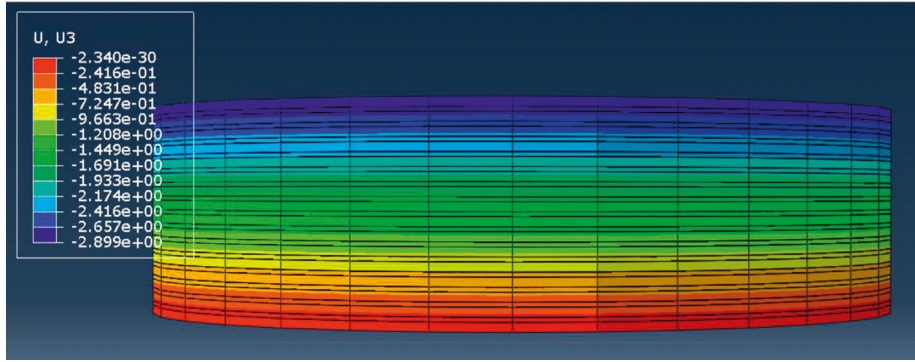
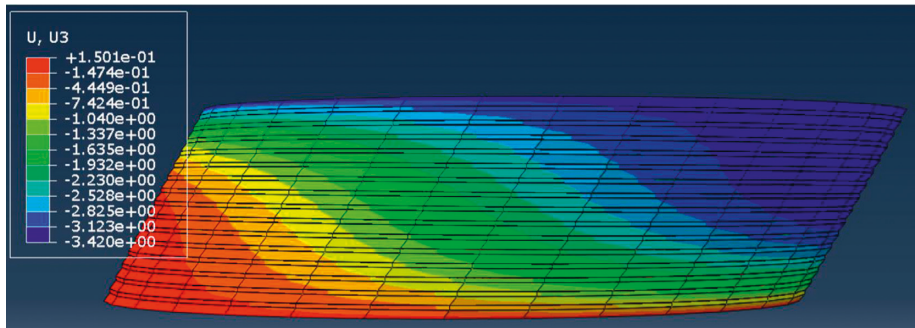FIGURE 21: The vertical displacement cloud of the bearing under pure pressure.

FIGURE 22: Vertical displacement cloud of the bearing when the horizontal displacement is 75 mm.
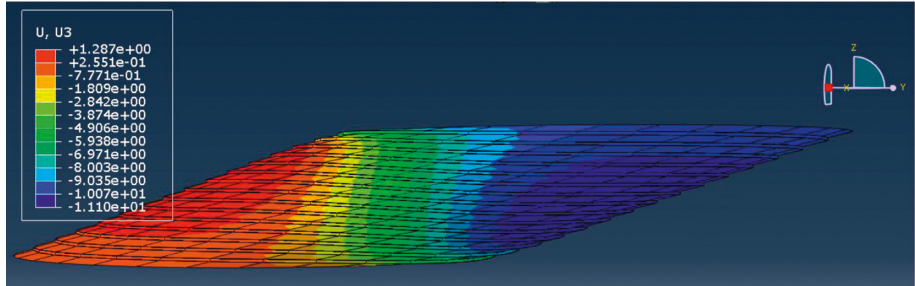

FIGURE 23: Vertical displacement cloud of the bearing under 400% ultimate compression shear.
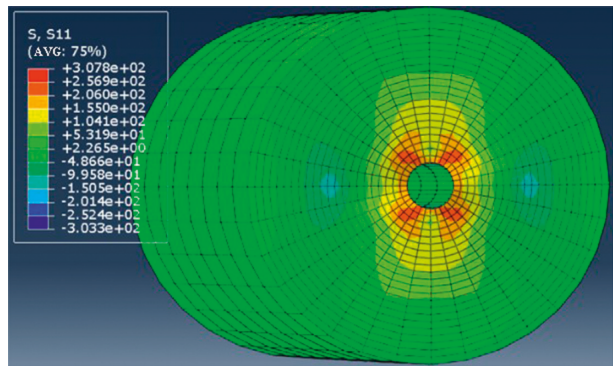

FIGURE 24: Stress cloud of middle layer S11 in 400% compression shear.

errors of both ETABS and ABAQUS software are relatively small and can be used simultaneously. The number of upper floors is 4, with a seismic isolation layer underneath and no designed basement. The height of the building structure is 15.6 m and the width is 28.1 m. The building structure is shown in Figure 34.
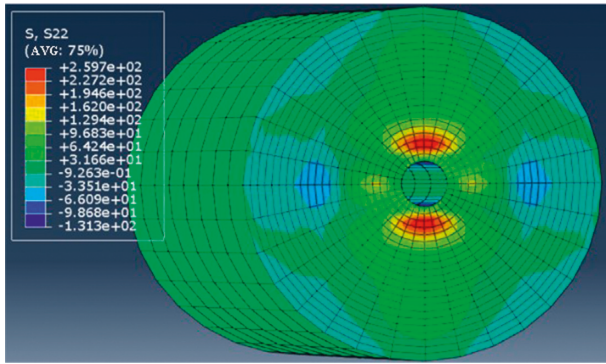
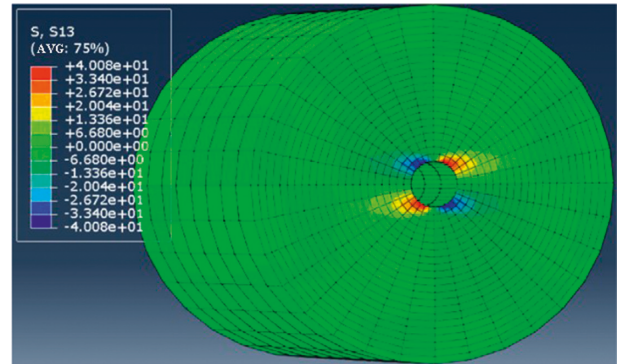Figure 25: Stress cloud of middle layer S22 in 400% compression shear.

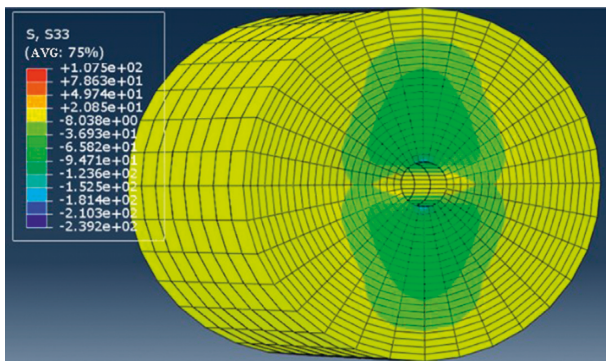Figure 28: Stress cloud of middle layer S13 in 400% compression shear condition.

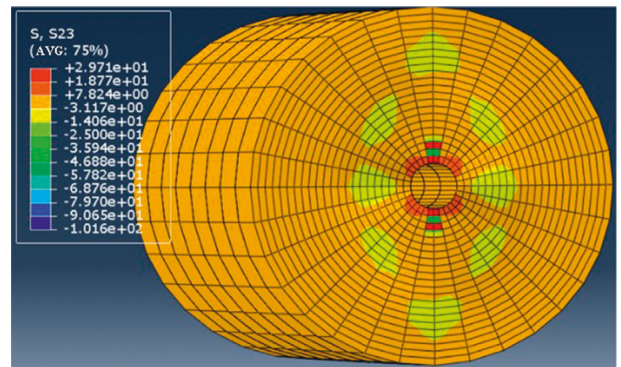Figure 26: Stress cloud of intermediate layer S33 in 400% compression shear condition.

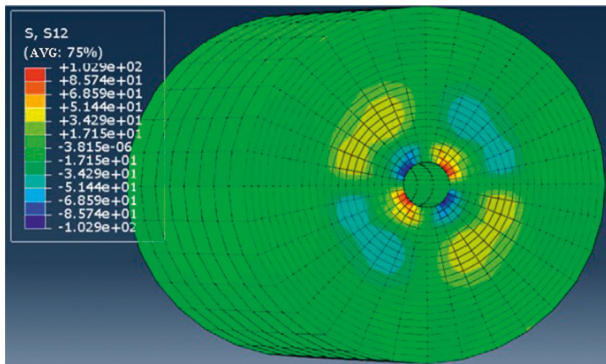Figure 29: Stress cloud of intermediate layer S23 in 400% compression shear condition.

Figure 27: Stress cloud of intermediate layer S12 in 400% compression shear condition.

Figure 30: Comparison of horizontal reaction force—horizontal displacement relationship curve.

In the engineering design, two artificial waves and five natural waves are generally selected for seismic waves, for a total of seven waves. The specific information of the selected seismic waves is in Tables 4 and 5. The seismic waves are shown in Figures 35 and 36. The side slope amplification factor is 1.1. Except for REN1 and REN2, which are artificial waves, the other five entries are all natural waves.

The seismic waves information is input into ETABS by defining the time course function.

The following two guidelines need to be followed for the seismic isolation design [15]: to take the expectation of a moderate earthquake at the site where the structure 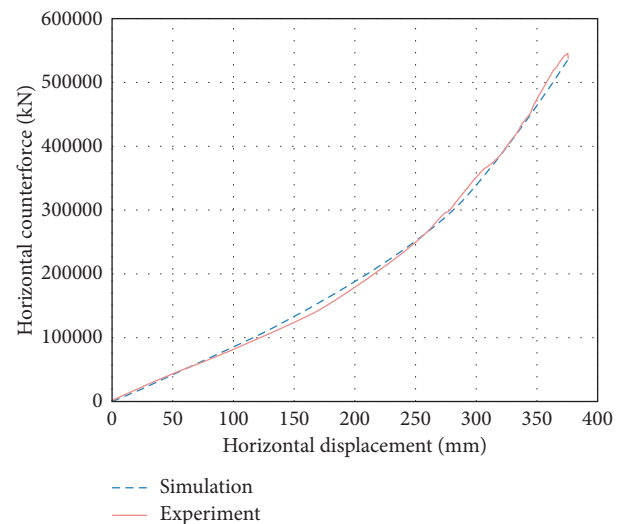is located during its lifetime as the basis for design; to take the most severe earthquake that may occur at the site as a test of structural safety, and to better study the deformation characteristics of the bearings when tensile stresses occur in
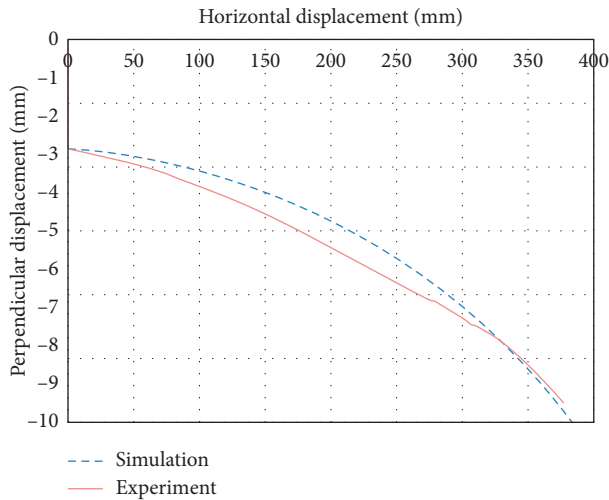
Figure 31: Comparison of vertical displacement-horizontal displacement relationship curve.
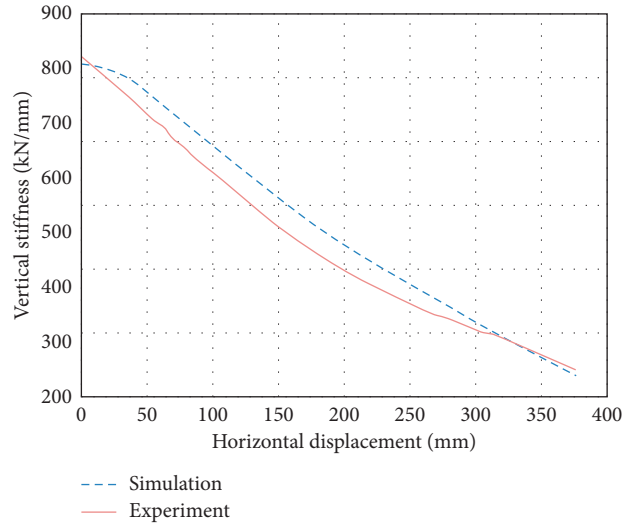

Figure 33: Comparison of vertical stiffness-horizontal displacement relationship curve.
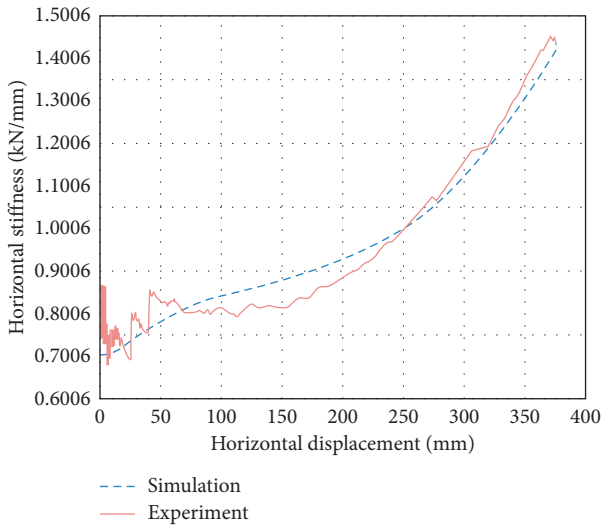

Figure 32: Comparison of horizontal stiffness-horizontal displacement relationship curve.

Figure 34: Floor model diagram.

the laminated rubber bearings, the bearings No. 3 and No. 25 were set as LNR500, for seismic isolation analysis. The design scheme is shown in Figure 37.

The eccentricity of the structure was first checked and the maximum eccentricity was 1.77% in Table 6, which satisfied the requirement.

Load combinations.

Combination (1): $1.0 \times$ representative value of gravity load $+ 1.0 \times$ horizontal earthquakes $- 0.5 \times$ vertical earthquakes.

Combination (2): $1.0 \times$ representative value of gravity load $- 1.0 \times$ horizontal earthquakes $- 0.5 \times$ vertical earthquakes.

Combination (3): $1.0 \times$ representative value of gravity load $+ 1.0 \times 45°$ horizontal earthquake $- 0.5 \times$ vertical earthquake.

Combination (4): $1.0 \times$ representative value of gravity load $+ 1.0 \times 225°$ horizontal earthquake $- 0.5 \times$ vertical earthquake.

The change in data is small because fewer bearings were changed, but due to the replacement of bearings, three more bearings produced positive axial forces, and No. 3 and No. 25 remained the bearings subjected to the greatest axial tension, and No. 3 was subjected to slightly greater tensile stress than No. 25.

This paper focuses on the analysis of the tensile situation of the seismic isolation bearing, so the force situation under the most unfavorable load combination of tensile

TABLE 4: Timing information table.

Abbreviation of time schedule	Full name of the time schedule	The maximum value of seismic acceleration is used for earthquake preparedness (cm/s²)	The maximum value of seismic acceleration is used for rare earthquakes (cm/s²)	Acquisition interval	Number of collection points
REN1	ACC5	200	400 ∗ 1.1	0.02	1501
REN2	RZ17	200	400 ∗ 1.1	0.02	1501
ELC	ELCENTRO	200	400 ∗ 1.1	0.02	1501
LWD	LWD_DEL AMO BLVD_90_nor	200	400 ∗ 1.1	0.02	1770
N90	NORTHRNWH090	200	400 ∗ 1.1	0.02	2000
N94	NGA_949NORTHR.ARL_FN	200	400 ∗ 1.1	0.02	1998
TAF	TAFT S69	200	400 ∗ 1.1	0.02	2720

TABLE 5: Duration schedule of the seven time course response spectra.

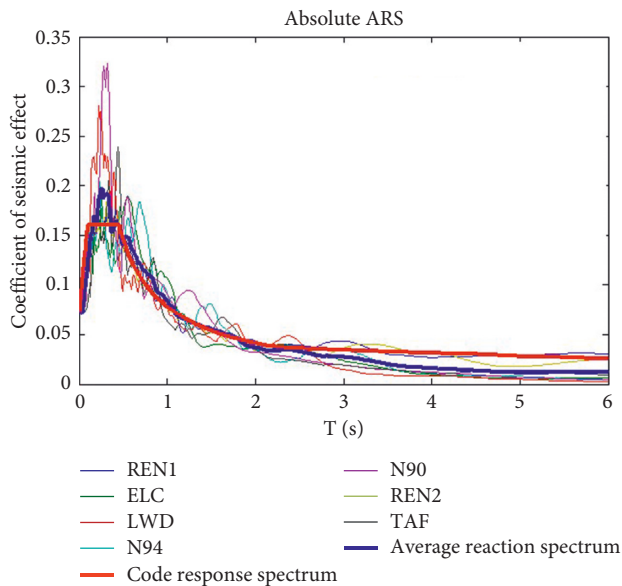| Schedule Name	The time corresponding to the first 10% of the maximum value of this seismic wave (S)	The time corresponding to 10% of the last time the maximum value of this seismic wave was reached (S)	Effective duration of the wave (S)	Structure cycle (S)	Ratio
REN1	2.020	23.100	21.08	2.437	8.7
REN2	0.540	17.440	16.90	2.437	6.9
ELC	0.861	29.174	28.313	2.437	11.6
LWD	0.037	33.638	33.601	2.437	13.8
N90	2.060	16.681	14.62	2.437	6.0
N94	2.180	24.180	22.00	2.437	9.0
TAF	1.048	45.398	44.35	2.437	18.2

FIGURE 35: 7 time course response spectra with canonical response spectra curves.

stress is mainly analyzed. By the table display function of the resultant data, the time course curve of the upper force of each bearing can be obtained. The model used in this section analyzes a total of 4 load combinations, and 7 waves are analyzed under each combination, each wave is divided into 2 cases of X- and Y-inputs, and there are 2 research bearings, No. 3 and No. 25. If the force conditions under each load combination of each bearing are all analyzed, there are 112 time curves in total, which is too many, so the representative ones should be selected as the research objects.

From Table 7, it is known that under the action of the rare earthquake, the maximum tensile stress of the bearing is 0.28 MPa in combination (1), which appears in bearing No. 3 LNR500; in combination (2), the maximum tensile stress of the bearing is 0.26 MPa, which appears in bearing No. 28 LNR500; when the horizontal earthquake is 45 degrees, the maximum tensile stress of the bearing is 0.25 MPa, which appears in bearing No. 3 When the horizontal earthquake is 225 degrees, the maximum tensile stress of the bearing is 0.25 MPa, which appears in No. 3 bearing LNR500. No. 3 and No. 25 are the same kind of bearing, but the tensile force at the location of No. 3 bearing is greater, so No. 3 bearing is the main object of study. The laminated rubber bearing selected for this study is a circular bearing, there is no bearing deformation characteristics related to the direction of deformation, so the four load combinations to select the relatively large upper force of the bearing combination (1).

In the load combination (1), the time-course curves of the force condition of No. 3 bearing are plotted in Figures 38–44.

Observing the above 14 sets of force time curves, it is obvious that the upper force of the bearing is greater when the seismic wave is input from the Y direction than when it is input from the X direction. Among the seven waves, REN1 and REN2 showed the largest fluctuations in the upper force of the bearing when they were input.

6. Analysis of the Results

The detailed seismic isolation analysis of this engineering case has been carried out by ETABS above, and the
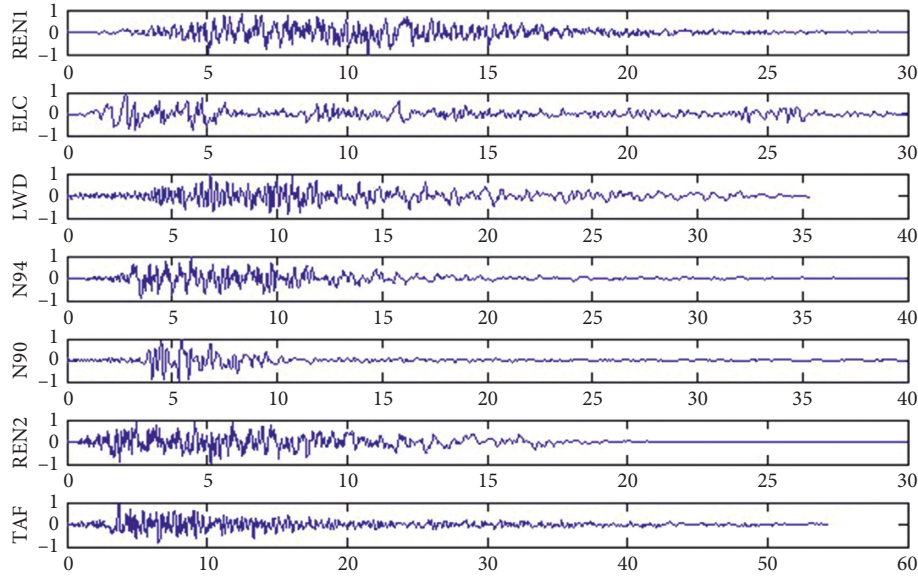
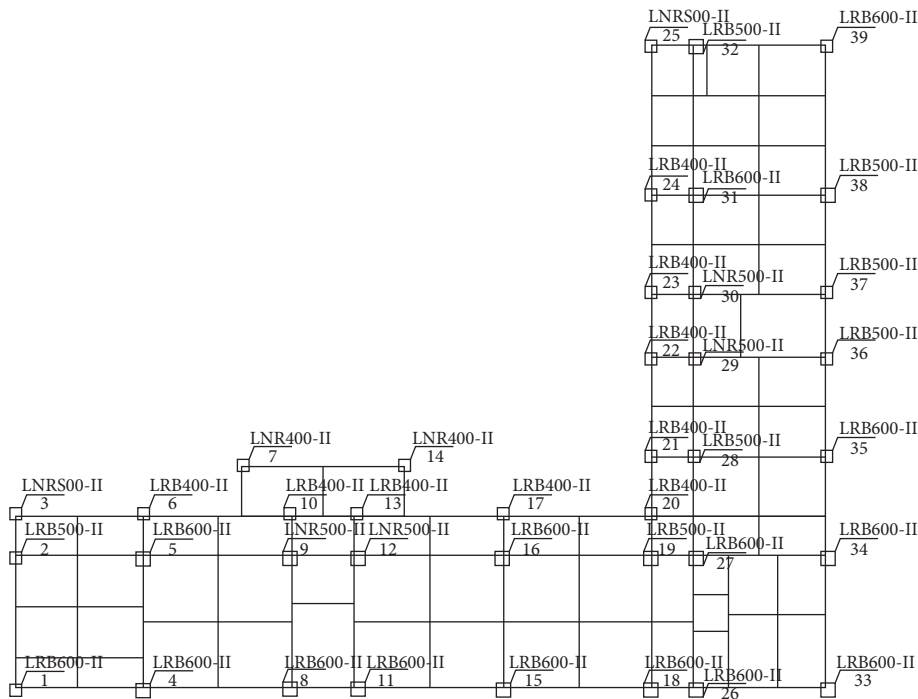FIGURE 36: Comparison of reaction spectrum and acceleration time curve.

FIGURE 37: Arrangement of bearing design.

TABLE 6: Eccentricity of seismic isolation structure.

Global coordinate	Center of gravity (m)	Rigid heart (m)	Eccentric distance (m)	Torsional stiffness (kN·m)	Stretch radius (m)	Eccentricity
X	31.61	31.39	0.35	18368102	19.54	1.09%
Y	12.33	12.67	0.21			1.77%

maximum horizontal displacement of the bearing in the seismic isolation layer does not exceed 250% of the thickness of the bearing rubber layer, within this range, the calculation error of ETABS and ABAQUS can be controlled within 10%,

so the analysis results above can be put into ABAQUS for a more accurate calculation of bearing No. 3.

The above total 14 force time curves, 7 of which have upper pressure greater than 0 and 7 of which do not exist, are inputted

TABLE 7: Maximum tensile stress and minimum axial force under different load combinations.

| Standoffs number	Stand model	Combination (1)		Combination (2)		Combination (3)		Combination (4)	
		Axial forcek (N)	Tensile stress (MPa)	Axial forcek (N)	Tensile stress (MPa)	Axial forcek (N)	Tensile stress (MPa)	Axial forcek (N)	Tensile stress (MPa)
1	LRB600	−79	−0.28	−80	−0.28	−71	−0.25	−71	−0.25
2	LRB500	−90	−0.46	−91	−0.46	−81	−0.41	−81	−0.41
3	LNR500	54	0.28	52	0.26	50	0.25	50	0.25
4	LRB600	−158	−0.56	−158	−0.56	−167	−0.59	−167	−0.59
5	LRB600	−220	−0.78	−220	−0.78	−215	−0.76	−215	−0.76
6	LRB400	−12	−0.09	−12	−0.09	−29	−0.23	−29	−0.23
7	LNR400	−21	−0.17	−21	−0.17	−17	−0.14	−17	−0.14
8	LRB600	−108	−0.38	−107	−0.38	−97	−0.34	−96	−0.34
9	LNR500	−112	−0.57	−112	−0.57	−106	−0.54	−106	−0.54
10	LRB400	−32	−0.25	−31	−0.25	−23	−0.18	−21	−0.17
11	LRB600	−108	−0.38	−107	−0.38	−93	−0.33	−93	−0.33
12	LNR500	−112	−0.57	−111	−0.57	−104	−0.53	−105	−0.54
13	LRB400	−31	−0.25	−30	−0.24	−24	−0.19	−22	−0.18
14	LNR400	−21	−0.17	−21	−0.16	−18	−0.14	−18	−0.14
15	LRB600	−146	−0.52	−145	−0.51	−161	−0.57	−161	−0.57
16	LRB600	−202	−0.72	−204	−0.72	−210	−0.74	−210	−0.74
17	LRB400	−21	−0.16	−19	−0.15	−39	−0.31	−38	−0.31
18	LRB600	−72	−0.25	−72	−0.26	−59	−0.21	−59	−0.21
19	LRB500	−94	−0.48	−95	−0.48	−101	−0.52	−103	−0.52
20	LRB400	−43	−0.34	−43	−0.35	−41	−0.32	−41	−0.33
21	LRB400	1	0.01	−1	−0.01	2	0.02	4	0.03
22	LRB400	3	0.03	1	0.01	1	0.00	0	0.00
23	LRB400	2	0.02	2	0.02	3	0.03	4	0.03
24	LRB400	−7	−0.06	−8	−0.06	−21	−0.17	−22	−0.17
25	LNR500	37	0.19	36	0.18	32	0.16	32	0.16
26	LRB600	−132	−0.47	−132	−0.47	−112	−0.40	−112	−0.40
27	LRB600	−188	−0.67	−187	−0.66	−205	−0.73	−206	−0.73
28	LRB500	−116	−0.59	−114	−0.58	−122	−0.62	−121	−0.61
29	LNR500	−103	−0.53	−104	−0.53	−95	−0.48	−96	−0.49
30	LNR500	−99	−0.50	−98	−0.50	−91	−0.47	−91	−0.46
31	LRB600	−193	−0.68	−192	−0.68	−191	−0.68	−190	−0.67
32	LRB500	−115	−0.59	−115	−0.59	−108	−0.55	−108	−0.55
33	LRB600	−104	−0.37	−103	−0.37	−91	−0.32	−91	−0.32
34	LRB600	−164	−0.58	−164	−0.58	−174	−0.62	−174	−0.62
35	LRB600	−90	−0.32	−90	−0.32	−99	−0.35	−99	−0.35
36	LRB500	−102	−0.52	−102	−0.52	−100	−0.51	−100	−0.51
37	LRB500	−97	−0.50	−97	−0.49	−95	−0.48	−95	−0.48
38	LRB500	−111	−0.57	−111	−0.56	−126	−0.64	−125	−0.64
39	LRB600	−81	−0.29	−81	−0.29	−71	−0.25	−71	−0.25
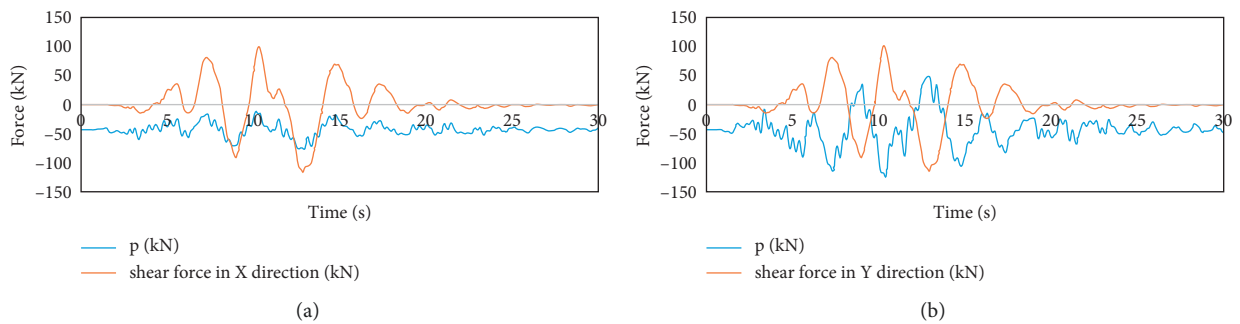
FIGURE 38: REN1 seismic waves under the bearing force time curve. (a) X-directional input. (b) Y-directional input.

into the LNR500 model that has been built in ABAQUS before in turn, after calculating the displacement, velocity and acceleration time curves of the bearing deformation in the earthquake. They are compared and analyzed to get what are the characteristics of the changes of the bearing in the cases where tensile stresses appear and those where they do not.
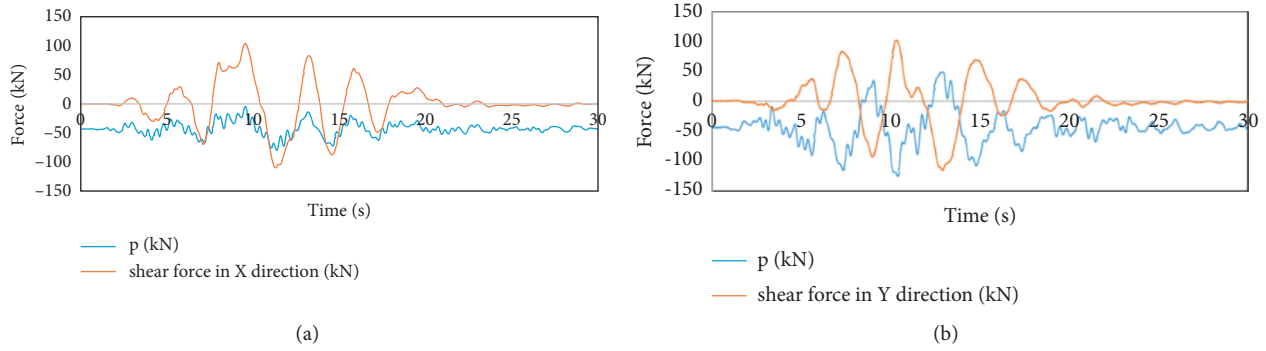
FIGURE 39: REN2 seismic waves under the bearing force time curve. (a) X-directional input. (b) Y-directional input.
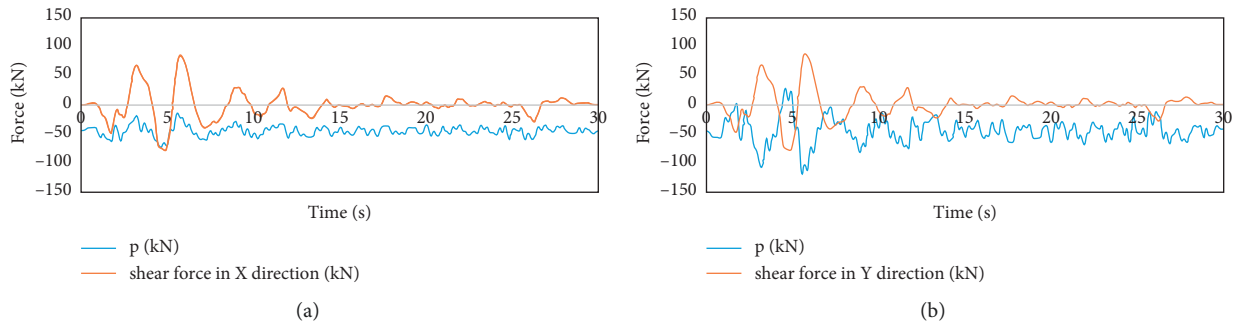

FIGURE 40: Time course curve of bearing force under ELC seismic wave. (a) X-directional input. (b) Y-directional input.
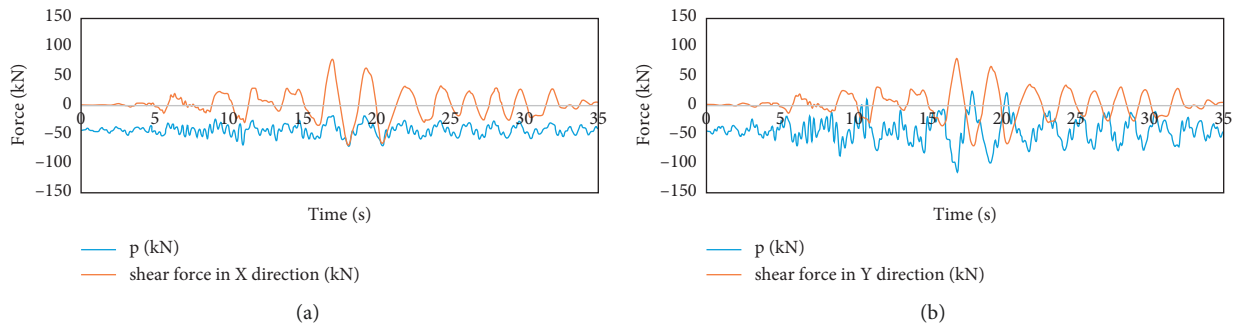

FIGURE 41: Time course curves of bearing stresses under LWD seismic waves. (a) X-directional input. (b) Y-directional input.
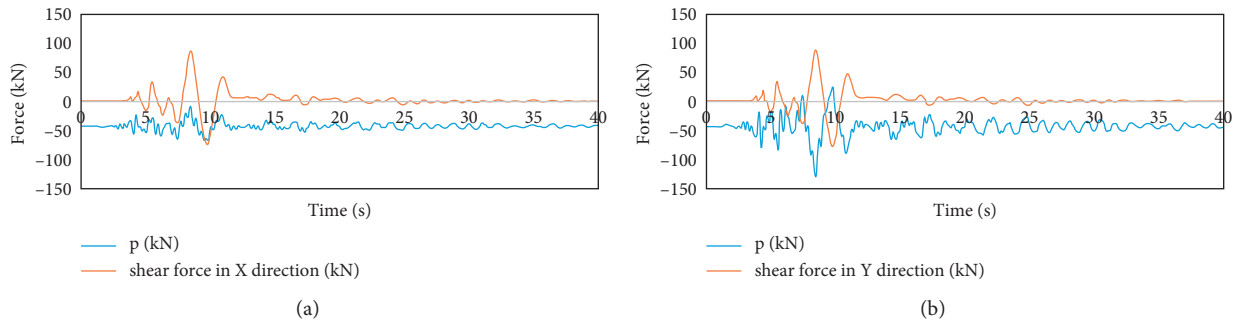

FIGURE 42: Time course curve of bearing force under N90 seismic wave. (a) X-directional input. (b) Y-directional input.
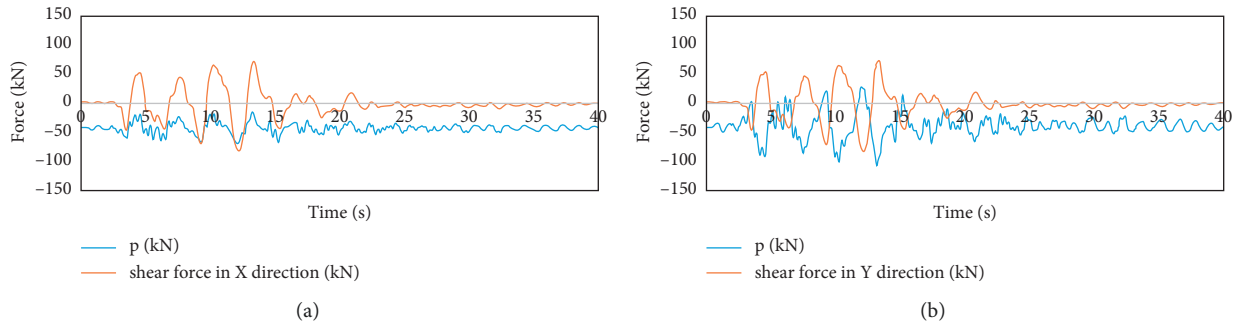
FIGURE 43: Time course curve of bearing force under N94 seismic wave. (a) X-directional input. (b) Y-directional input.
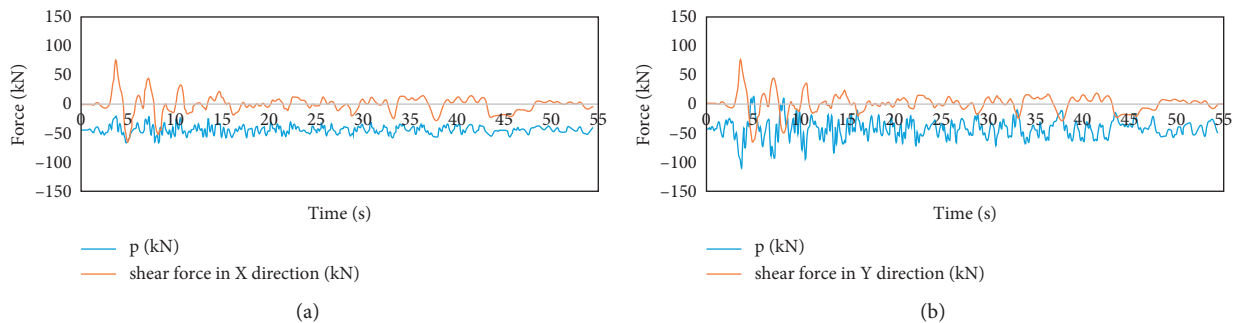

FIGURE 44: Time course curves of bearing stresses under TAF seismic waves. (a) X-directional input. (b) Y-directional input.

In order to observe the connection between displacement, velocity and acceleration of bearing deformation more intuitively, the displacement, velocity and acceleration time curves were drawn on one graph, as shown in Figures 45–58. However, since they are not of one order of magnitude, especially the acceleration is generally relatively large. Therefore, when drawing the graph, the acceleration needs to be reduced by a certain multiple, and the vertical displacement also has a smaller value, so it needs to be enlarged by a certain multiple. For example, in the horizontal deformation in Figure 45, the acceleration unit is labelled as $20 \, mm/s^2$, which means the acceleration is reduced by 20 times; while in the vertical deformation in Figure 45, the displacement unit is labelled as 0.5 mm, which means the displacement is enlarged by 2 times.

In ABAQUS, a total of 14 sets of dynamic analysis were done, and the above 28 sets of time-course curves were obtained. In each set of curves, the highest frequency of change was acceleration, followed by velocity, and the lowest was displacement.

This paper is prepared for the reference of the tensile device, so in the exploration of the first to define under what circumstances to determine the bearing in the tensile situation, in order to determine when the bearing is in what condition when the tensile device needs to play a role. In this paper, the laminated rubber bearing tension not only need to consider the upper bearing pressure less than 0, but also need to consider the horizontal displacement of the larger case, the simulation results in preceding paragraphs found that the LNR500 horizontal displacement of 75 mm that is, the horizontal shear of 81.5% or so, the bearing should start

to have local tension, after reaching 150%, the bearing tension is more obvious, comprehensive Considering, this paper considers that when the upper pressure of the bearing is positive and the horizontal displacement of the bearing is greater than 200% of the thickness of the rubber layer, i.e. 186 mm, the bearing is considered to be in tension.

Observation and comparison of the above graphs will show that when the displacement of the bearing deformation is relatively large, its velocity in the adjacent time period is also larger, but the acceleration is not necessarily larger, in this case most of the time course curve changes are characterized by a smaller acceleration in a certain time period, its nearby displacement is larger. And the load combination with larger maximum displacement, its corresponding maximum acceleration is not necessarily proportional, take the two different cases of REN2's X-direction input and Y-direction input as an example, it is known from the previous subsection that the upper force of the bearing is larger when Y-direction input, and there is the case that the upper vertical force is positive. Horizontal acceleration is $9.81 \, mm/s^2$, maximum vertical displacement is 0 mm, and maximum vertical acceleration is $0.59 \, m/s^2$; when REN2 is input from Y direction, the maximum horizontal displacement corresponding to bearing deformation is 109.57 mm, maximum horizontal acceleration is $6.85 \, mm/s^2$, maximum vertical deformation is 0.09 mm, and maximum vertical acceleration is also $0.59 \, m/s^2$. input horizontal displacement is 5.59% larger than the maximum horizontal displacement in Y direction input, but its maximum horizontal acceleration is 43.21% larger; the vertical displacement in Y direction input is obviously larger, but its maximum vertical acceleration is the same.
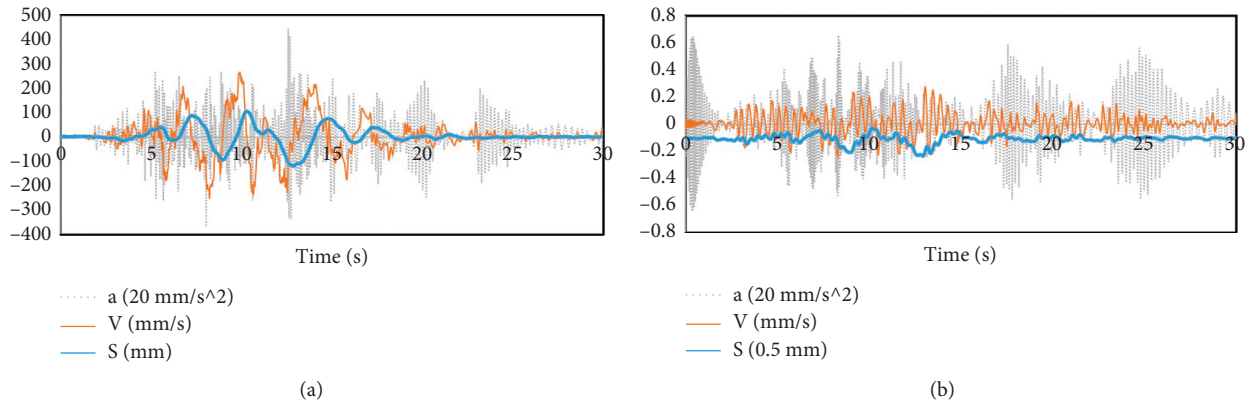
(a)

(b)

FIGURE 45: Time course curves of displacement, velocity and acceleration of bearing deformation when REN1 is input from X direction. (a) Horizontal deformation. (b) Vertical deformation.
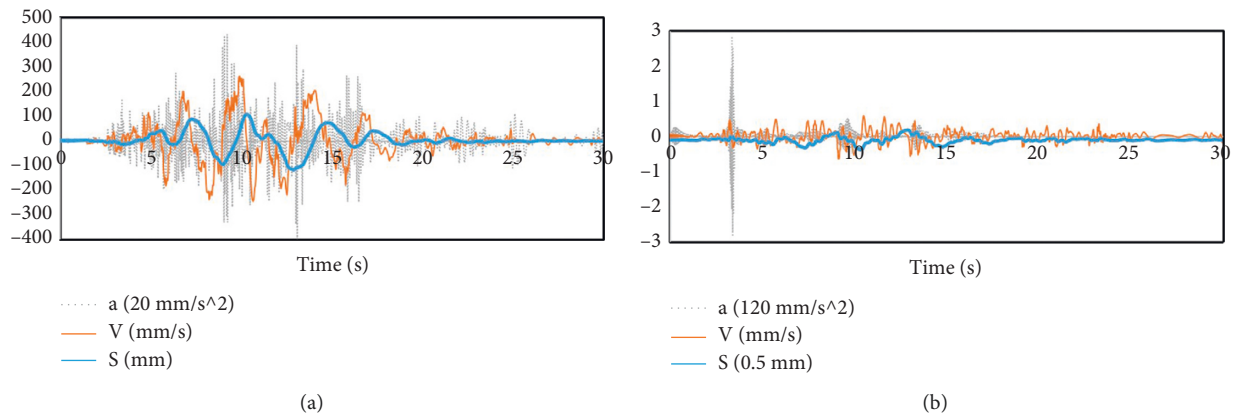

(a)

(b)

FIGURE 46: Time course curves of displacement, velocity and acceleration of bearing deformation when REN1 is input from Y direction. (a) Horizontal deformation. (b) Vertical deformation.
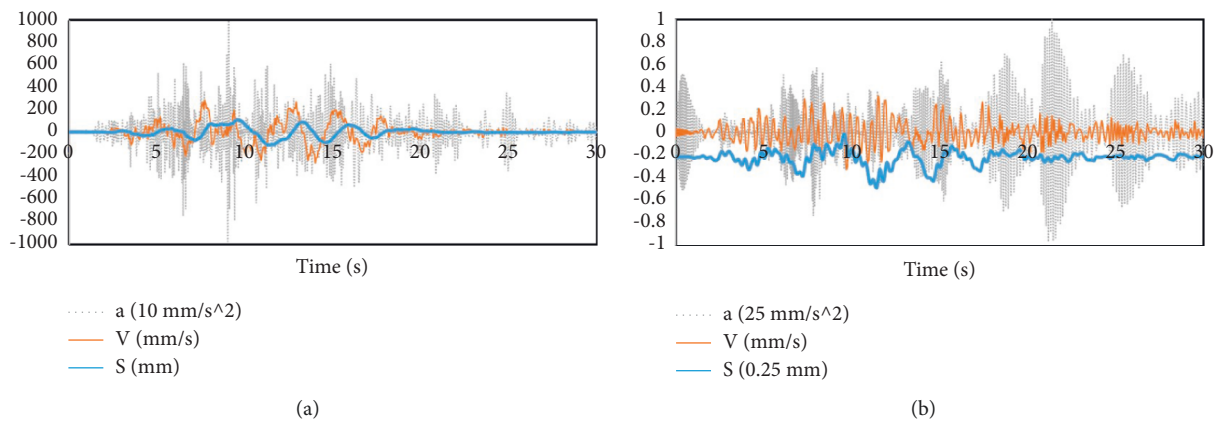

(a)

(b)

FIGURE 47: Time course curves of displacement, velocity and acceleration of bearing deformation when REN2 is input from X direction. (a) Horizontal deformation. (b) Vertical deformation.

Such deformation characteristics may not be conducive to the role of acceleration-controlled tensile devices, but the use of velocity-controlled tensile devices can be considered. As the case model used in this paper is small, the horizontal displacement and vertical displacement of the bearing are not particularly large, and when the horizontal displacement is close to 200% of the thickness of the rubber layer and the vertical displacement is greater than 0, the maximum velocity near its corresponding position is close to 350 mm/s. Therefore,
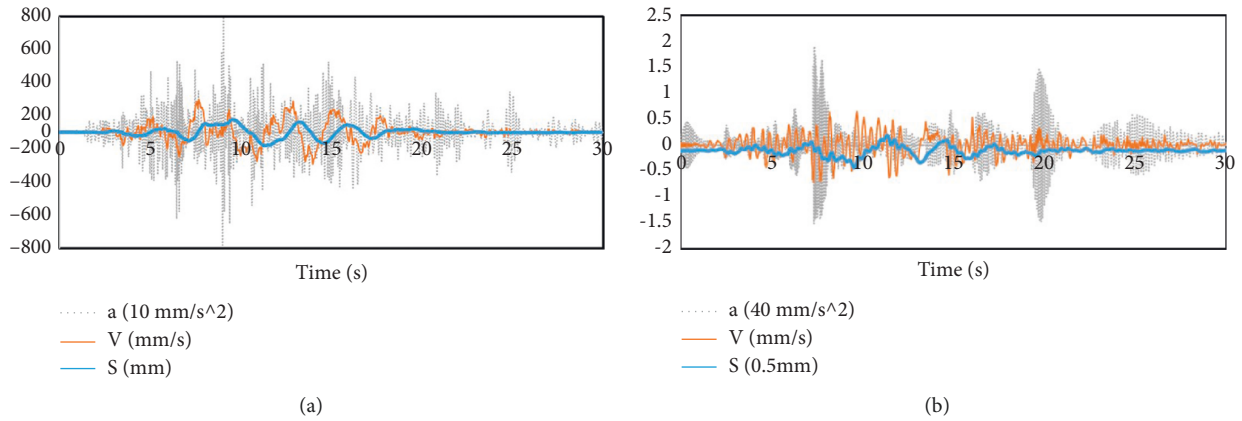
(a)

(b)

FIGURE 48: Time course curves of displacement, velocity and acceleration of bearing deformation when REN2 is input from *Y* direction. (a) Horizontal deformation. (b) Vertical deformation.
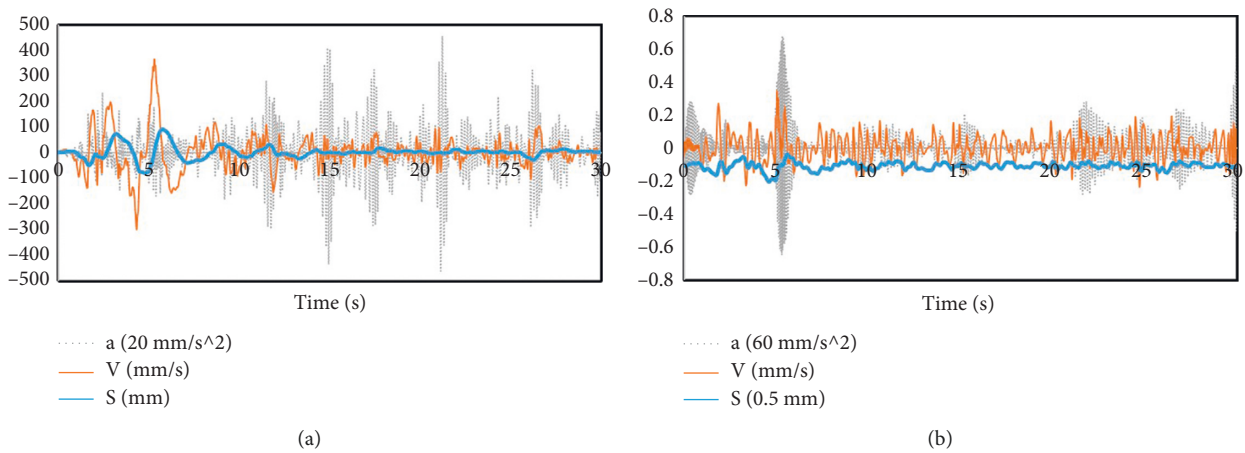

(a)

(b)

FIGURE 49: Time course curves of bearing deformation displacement, velocity and acceleration when ELC is input from *X* direction. (a) Horizontal deformation. (b) Vertical deformation.
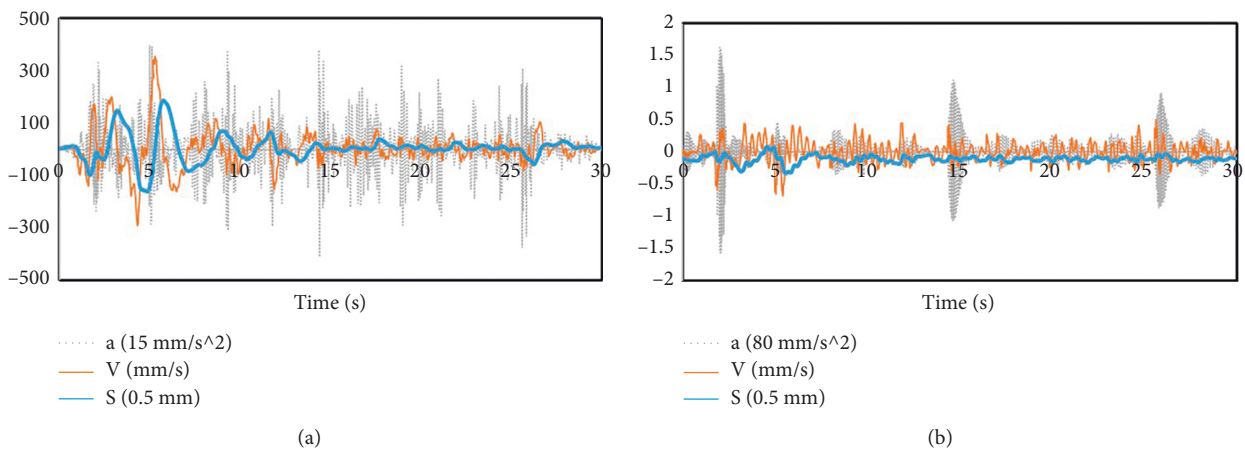

(a)

(b)

FIGURE 50: Time course curves of bearing deformation displacement, velocity and acceleration when ELC is input from *Y* direction. (a) Horizontal deformation. (b) Vertical deformation.

(a)

(b)

FIGURE 51: Time course curves of bearing deformation displacement, velocity and acceleration when LWD is input from *X* direction. (a) Horizontal deformation. (b) Vertical deformation.
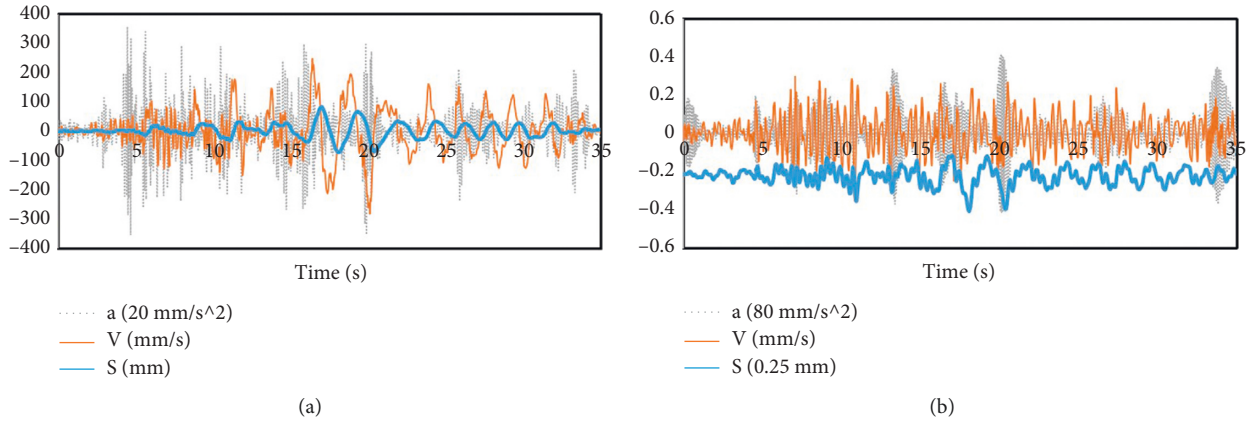

(a)

(b)

FIGURE 52: Time course curves of bearing deformation displacement, velocity and acceleration when LWD is input from *Y* direction. (a) Horizontal deformation. (b) Vertical deformation.

(a)

(b)

FIGURE 53: Time course curves of bearing deformation displacement, velocity and acceleration when N90 is input from *X* direction. (a) Horizontal deformation. (b) Vertical deformation.
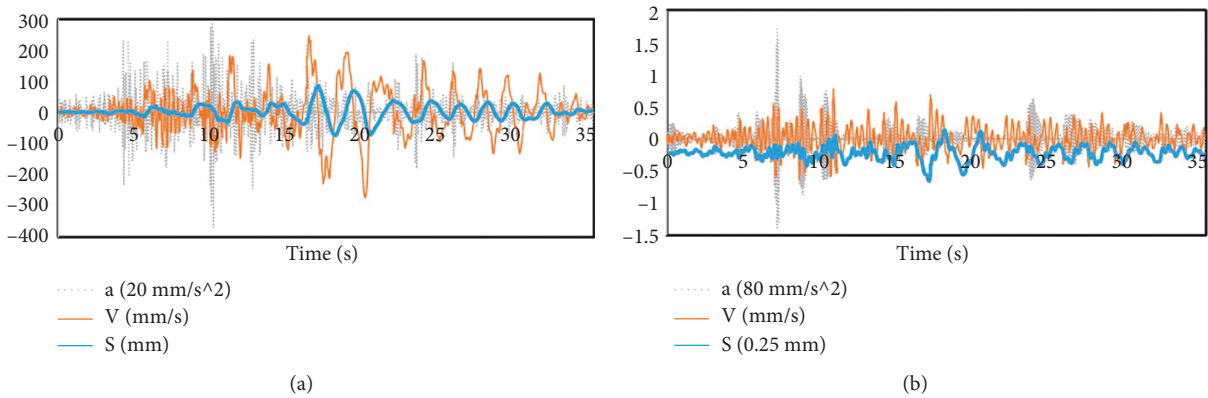
considering all aspects, this paper believes that the velocity-controlled tensile device of LNR500 can be considered to set the action velocity at 400 mm/s (0.4 m/s), that is, when the bearing deformation speed reaches 0.4 m/s, the tensile device then starts to play the tensile effect.
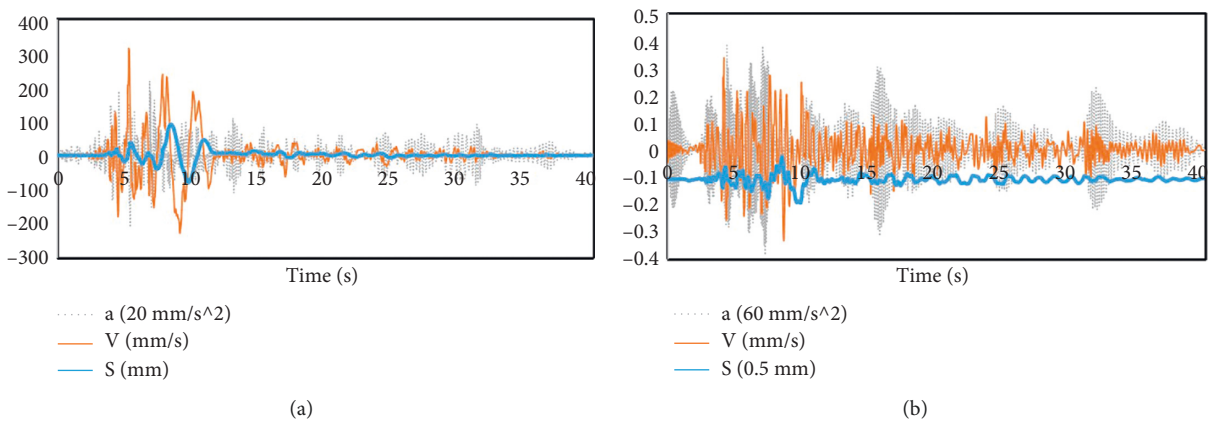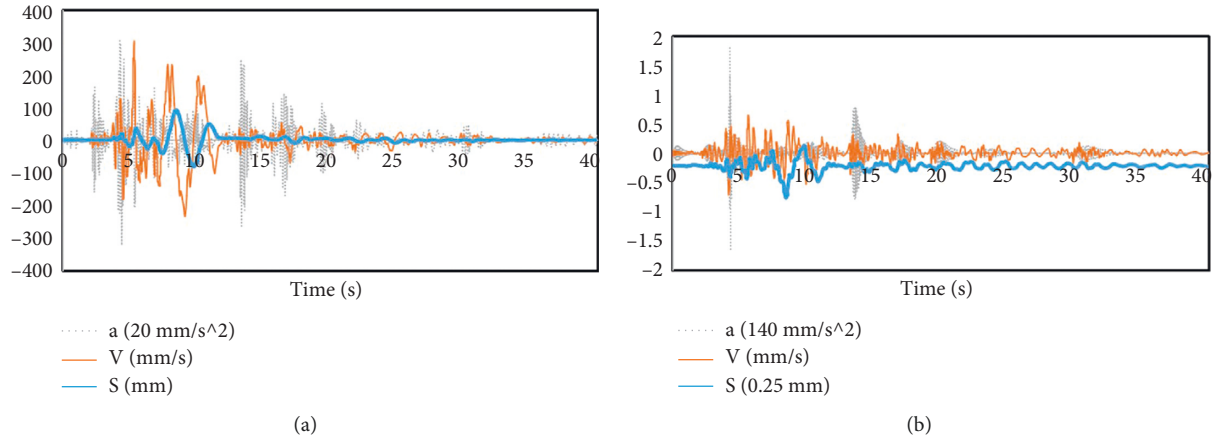
(a)

(b)

FIGURE 54: Time course curves of bearing deformation displacement, velocity and acceleration when N90 is input from Y direction. (a) Horizontal deformation. (b) Vertical deformation.

(a)

(b)
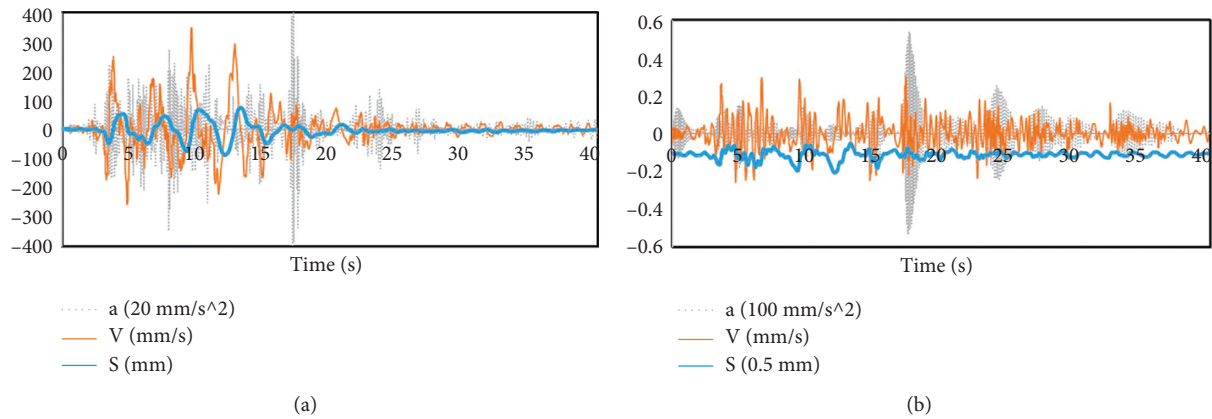
FIGURE 55: Time course curves of bearing deformation displacement, velocity and acceleration when N94 is input from X direction. (a) Horizontal deformation. (b) Vertical deformation.

(a)

(b)

FIGURE 56: Time course curves of bearing deformation displacement, velocity and acceleration when N94 is input from Y direction. (a) Horizontal deformation. (b) Vertical deformation.

FIGURE 57: Time course curves of bearing deformation displacement, velocity and acceleration when TAF is input from *X* direction. (a) Horizontal deformation. (b) Vertical deformation.

FIGURE 58: Time course curves of bearing deformation displacement, velocity and acceleration when TAF is input from *Y* direction. (a) Horizontal deformation. (b) Vertical deformation.
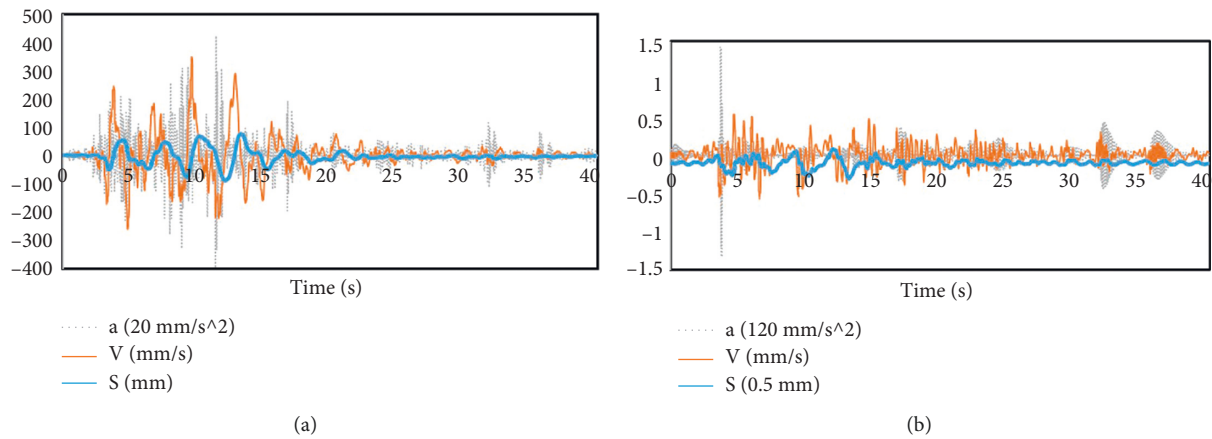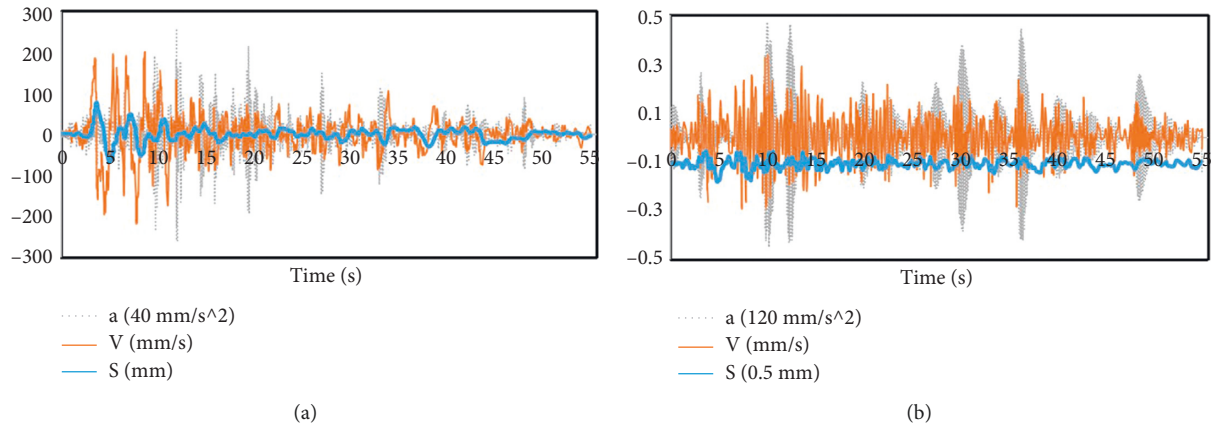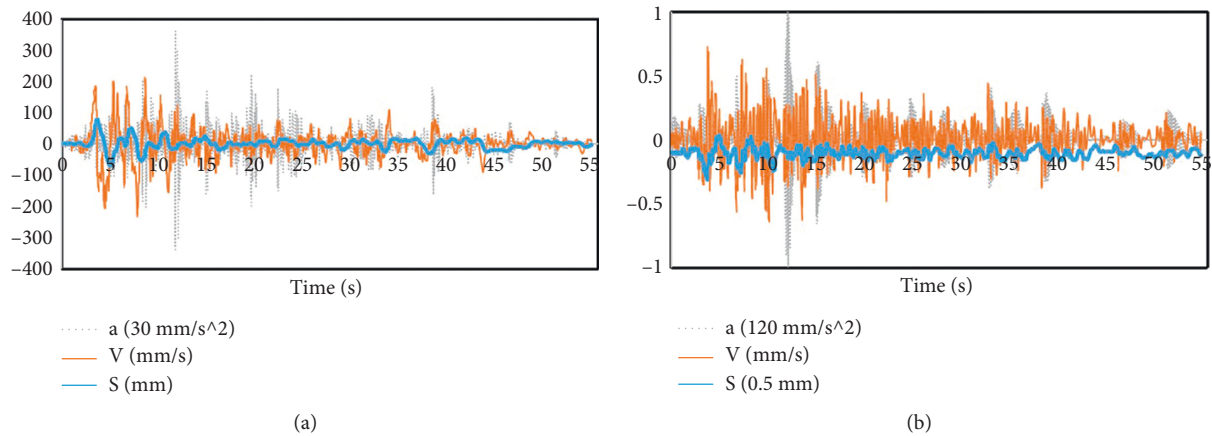
7. Conclusion

With the increase of seismically isolated buildings, the weakness of poor tensile capacity of seismic isolation bearings is also increasingly highlighted. For this reason, the design research of seismic isolation bearing tensile devices is also emerging. However, the deformation of the bearing itself in the earthquake process is relatively complex, and its deformation characteristics will have certain influence on the performance of the tensile device. In order to study the tensile device more reasonably and make the research results more reliable, the deformation characteristics of the seismic isolation bearing should be studied more thoroughly first. In this paper, three sets of materiality tests, 400% compression shear test of LNR500 bearing and 400% compression shear test of LNR500 bearing were firstly conducted; the materiality parameters obtained from the tests were applied, and the static analysis of the correlation between vertical displacement and horizontal displacement was carried out on LNR500 bearings with finite element analysis software, and the relationship curves between horizontal stiffness of the bearing and vertical stiffness and horizontal displacement of

the bearing were obtained. The relationship curves between the horizontal stiffness and vertical stiffness of the bearing and the horizontal displacement of the upper part of the bearing were obtained; seismic isolation analysis was carried out for an actual engineering case, and the results of the upper force time course of the bearing were imported into ABAQUS software, and dynamic analysis was carried out for LNR500 to obtain the displacement, velocity and acceleration time course curves of the horizontal and vertical deformation of the bearing. After the comprehensive analysis, the following conclusions were obtained.

(1) When the bearing is in compression-shear state, the bearing's compressed area will be reduced because of the increase of the upper horizontal displacement, resulting in the reduction of the vertical stiffness of the bearing, thus increasing the vertical displacement, so this part of the displacement should be taken into account when designing the tensile device to guarantee the vertical clearance. In general, the maximum horizontal displacement of the bearing in the seismic isolation structure under the action of earthquake does not exceed 250% of the thickness of

the rubber layer, corresponding to the tensile device of LNR500 should retain the vertical clearance of 5 mm.

(2) In the simulation of large deformation of rubber bearing, Yeoh and Ogden models are commonly used, and Yeoh model is used in this paper. Usually in the bearing finite element simulation, rubber is often assumed to be incompressible model, this paper also simulates the compression model and incompressible model in the simulation, the results show that the vertical stiffness of the incompressible model of the bearing is larger, the numerical analysis results and test results are very big difference; and the horizontal stiffness of the incompressible model simulation is also larger than the compressible model, and the error will increase with the increase of horizontal displacement, when the horizontal displacement is greater than 320% of the thickness of the rubber layer, the relative error of the two horizontal stiffnesses is more than 10%. Therefore, in the simulation modeling stage of the research process of tensile device, the rubber should use compressible model.

(3) The vertical stiffness and horizontal stiffness of the laminated rubber bearing will change with the change of horizontal displacement of the upper part of the bearing, and the change has the following law (the correlation can also be established by the method of this paper for bearings of different materials or different diameters): the vertical stiffness of the bearing decreases nearly linearly with the increase of horizontal displacement is about 1.55 kN/mm^2.

(4) The research and design analysis of the speed-controlled tensile device and acceleration-controlled tensile device show that when the LNR500 deformation displacement is large and the tensile force is large, the acceleration in the adjacent time period is usually small, and this deformation characteristic is not conducive to the acceleration-controlled tensile device to play its role, so it is not recommended to use; and there is generally a large change speed in this time period, and this speed is about 0.4 m/s, so it is recommended that the velocity-controlled tensile device designed for LNR500 should be designed to act at a velocity of 0.4 m/s.

The types of tensile devices can be roughly divided into three categories: displacement controlled tensile devices, speed controlled tensile devices and acceleration controlled tensile devices. The static analysis is mainly for the displacement controlled tensile device, and the dynamic analysis is mainly for the speed controlled tensile device and the acceleration controlled tensile device. The research results of this paper provide some reference data for the design research of LNR500 tensile device, and also provide some research ideas for the tensile devices of other bearings in the future. However, the static and dynamic analysis of the laminated rubber bearing is carried out in this paper, but it

mainly assumes the state of the floor without overturning, under this state, the vertical displacement of the bearing is small, and the reference significance of its deformation is more limited. If we want to better explore the deformation characteristics of the bearing when it is under tension in the earthquake, we should find a large engineering case with a larger aspect ratio to do the analysis, and take the overturning displacement into consideration.

Data Availability

The dataset can be accessed upon request.

Conflicts of Interest

The authors declare that they have no conflicts of interest regarding this work.

Acknowledgments

References

[1] H. Yu-xian, *Earthquake Engineering*, Seismological Press, China, 2006.

[2] J. M. Kelly, "Experimental results of an earthquake isolation system using natural rubber bearing," Report No.UCB/EERC-78/03, University of California, California, CA,USA, 1978.

[3] C. Peng, Y. Zhou, L. Lu, L. Jiang, K. Hu, and G. Qu, "Experimental reseaerch on mechanical performance of tension-resistant device for rubber bearings," *Jouranl of building structures*, vol. 38, no. 7, pp. 113–119, 2017.

[4] X. Yan, Y. Zhang, H. Wang, and W. Lushun, "Shaking table test for the sturcture with three-dimensional base isolation and overturn resistance devices," *Engineering Mechanics*, vol. 27, no. 5, pp. 91–96, 2010.

[5] C. G. Koh and J. M. Kelly, "A simple mechanical model for elastomeric bearings used in base isolation," *International Journal of Mechanical Sciences*, vol. 30, no. 12, pp. 933–943, 1988.

[6] J. M. Kelly, *Earthquake-resistant Design with Rubber*, Springer-Verlag, London, 1997.

[7] X. Li and X. Yang, "A review of elastic constitutive model for rubber materials," *China Elastomerics*, vol. 15, no. 1, pp. 52–60, 2005.

[8] W. Wang, T. Deng, and S. Zhao, "Determination for material constants of rubber Mooney-Rivlin model," *Special purpose rubber products*, vol. 25, no. 4, pp. 8–10, 2011.

[9] O. H. Yeoh, "Characterization of elastic properties of carbon-black-filled rubber vulcanizates," *Rubber Chemistry and Technology*, vol. 63, no. 5, pp. 792–805, 1990.

[10] O. H. Yeoh, "Some forms of the strain energy function for rubber," *Rubber Chemistry and Technology*, vol. 66, no. 5, pp. 754–771, 1993.

[11] R. W. Ogden, "Large deformation isotropic elasticity: on the correlation of the theory and experiment for compressible rubberlike solids," *Proceedings of Royal Society of London Series A*, vol. 328, pp. 567–583, 1972.

[12] J. Wang, P. Guan, and Q. Yao, "Analysis of bilateralseism iceresponse of base-isolated structures with lead rubber

bearings," *Earthquake Engineering and Engineering Vibration*, vol. 25, no. 1, pp. 133–137, 2005.

[13] M. Ohsaki, T. Miyamura, M. Kohiyama, T. Yamashita, M. Yamamoto, and N. Nakamura, "Finite-element analysis of laminated rubber bearing of building frame under seismic excitation," *Earthquake Engineering & Structural Dynamics*, vol. 44, no. 11, pp. 1881–1898, 2015.

[14] X. Luo, "The relation between simple shear and pure shear in rubber," *Acta Polymerica Sinica*, vol. 1994, no. 4, pp. 385–391, 1994.

[15] A. Li, *Vibration Control for Building Structures: Theory and Applications*, Springer, Berlin, Germany, 2020.